nature reviews materials

https://doi.org/10.1038/s41578-025-00860-9

Review article

Check for updates

Symmetry-driven artificial phononic media

Simon Yves[1], Michel Fruchart[2], Romain Fleury[3], Gal Shmuel[1,4], Vincenzo Vitelli[5,6], Michael R. Haberman[7] ✉ & Andrea Alù[1,8] ✉

Abstract

Phonons are quasiparticles associated with mechanical vibrations in materials. They are at the root of the propagation of sound and elastic waves, as well as of thermal phenomena, which are pervasive in our everyday life and in many technologies. The fundamental understanding and control of phonon responses in natural and artificial media are key in the context of communications, isolation, energy harvesting and control, sensing and imaging. It has recently been realized that controlling different symmetry classes at the microscopic and mesoscopic scales in synthetic media offers a powerful tool to precisely tailor phononic responses for advanced acoustic and elastodynamic wave control. In this Review, we survey the recent progress in the design and synthesis of artificial phononic media, namely phononic crystals and metamaterials, guided by symmetry principles. Starting from tailored broken spatial symmetries, we discuss their interplay with time symmetries for non-reciprocal and non-conservative phenomena. We also address broader concepts that combine multiple symmetry classes to induce exotic phononic wave transport. We conclude with an outlook on future research directions based on symmetry engineering for the advanced control of phononic waves.

Sections

[1]Photonics Initiative, Advanced Science Research Center, City University of New York, New York, NY, USA. [2]Gulliver, CNRS, ESPCI Paris, Université PSL, Paris, France. [3]Laboratory of Wave Engineering, EPFL, Lausanne, Switzerland. [4]Faculty of Mechanical Engineering, Technion-Israel Institute of Technology, Haifa, Israel. [5]James Franck Institute, University of Chicago, Chicago, IL, USA. [6]Kadanoff Center for Theoretical Physics, University of Chicago, Chicago, IL, USA. [7]Walker Department of Mechanical Engineering, The University of Texas at Austin, Austin, TX, USA. [8]Physics Program, Graduate Center, City University of New York, New York, NY, USA. ✉e-mail: haberman@utexas.edu; aalu@gc.cuny.edu

Introduction

As outlined by Pierre Curie in the late nineteenth century[1], symmetries play a fundamental role in the physical understanding of various natural phenomena, especially in the context of wave behaviour. As a consequence, physicists and engineers have been hunting for the presence or absence of symmetries in systems not only to understand, but also to tailor their physical properties. In this Review, we provide a unified perspective on the latest research on the propagation of mechanical waves in mesostructured materials, such as phononic crystals and metamaterials, under the paradigm of symmetries and symmetry breaking. Recent reviews of acoustic and elastic metamaterials and metasurfaces[2–6] feature exciting advances in the control of mechanical wave propagation through structured media. Here, we aim at articulating this progress across different classes of symmetry engineering, showing how this approach can provide a powerful perspective to understand, design and optimize phononic metastructures.

Overall, the concept of symmetry is very general: it includes any transformation that keeps an object unchanged. This is the case for the familiar spatial symmetries, which we discuss after introducing some basic phononics concepts. We then expand to abstract symmetries connected to the temporal evolution of a system, including reciprocity, time-reversal, time-translation invariance and energy conservation. Finally, we discuss generalized symmetries involving families of systems such as dualities and twist symmetries (Fig. 1).

Symmetry-driven phononics in a nutshell

Mechanical waves and how they propagate

In this Review, we focus on elastic waves (mechanical waves in solids) and acoustic waves (mechanical waves in fluids and gases). Possibly the simplest description of mechanical waves is from the perspective of continuum theories[7–10]. For instance, acoustic waves in a simple fluid can be captured by the acoustic wave equation

$$\beta\partial_t^2 p = \rho_0^{-1}\nabla^2 p, \tag{1}$$

where $p(t,\mathbf{r})$ is the pressure, ρ_0 the density of the unperturbed fluid and β its isentropic compressibility (the inverse of the isentropic bulk modulus $B = \beta^{-1}$). This equation can be obtained by linearizing the Navier–Stokes equations along with an isentropic equation of state[9,11].

Similarly, continuum elasticity describes the propagation of elastic waves in an ideal, uniform and isotropic solid by the equation of motion[10,12]

$$\rho\partial_t^2\mathbf{u} = \mu\nabla^2\mathbf{u} + \left(B + \frac{\mu}{3}\right)\nabla(\nabla\cdot\mathbf{u}), \tag{2}$$

in which ρ is the mass density of the solid, $\mathbf{u}(t,\mathbf{r})$ the displacement field that measures the motion of the solid with respect to a reference configuration, and μ and B are the shear and bulk moduli, respectively. Both equations (1) and (2) can be traced to conservation laws that arise from symmetry: the conservation of mass $\partial_t\rho + \rho\nabla\cdot\mathbf{v} = 0$ and the conservation of linear momentum $\partial_t\boldsymbol{\mu} = \nabla\cdot\boldsymbol{\sigma} + \mathbf{f}$, in which $\boldsymbol{\mu} = \rho\mathbf{v}$ is the density of linear momentum, $\mathbf{v} = \partial_t\mathbf{u}$ the velocity field, $\boldsymbol{\sigma}$ the stress tensor, and $\mathbf{f}$ the density of body forces applied externally (set to zero here). Acoustic waves are longitudinal, whereas elastic waves include both longitudinal compression waves and transverse shear waves. Both acoustic and elastic waves have a polarization (the direction of the oscillating velocity or displacement field, respectively), which can be, in the case of plane waves, related to their longitudinal or transverse nature[13].

Equations (1) and (2) may not be sufficient to describe wave propagation. This can happen when the material does not satisfy the required symmetries, if there are other degrees of freedom in the system, if the system exhibits nonlinearities or if a continuum theory is not appropriate given the size of material heterogeneities of the medium when compared with the wavelength. Several of these conditions may apply at the same time, especially in the context of engineered materials.

Materials with lower symmetries

When mechanical waves propagate in materials with lower symmetries, the propagation equations typically acquire additional terms accounting for new couplings between degrees of freedom that arise when the symmetry of the system is reduced. It can happen that the equations keep roughly the same form but are more complicated. For instance, a more general version of equation (2) that does not assume isotropy reads (neglecting body forces)

$$\rho\partial_t^2 u_i = \partial_j[C_{ijk\ell}\partial_\ell u_k], \tag{3}$$

in which u_i is the ith Cartesian component of $\mathbf{u}$, and $\partial_i \equiv \partial/\partial r_i$ are partial derivatives with respect to space. Here, $C_{ijk\ell}$ is the elasticity tensor, which relates the stress σ_{ij} to the displacement gradients $\partial_\ell u_k$ through $\sigma_{ij} = C_{ijk\ell}\partial_\ell u_k$. Compared with equation (2), more terms are present, but they are roughly of the same type (a second-order derivative with respect to space). Any remaining symmetry is encoded in $C_{ijk\ell}$. For instance, spatial symmetries represented by matrices $U \in O(d)$ constrain the elastic tensor through $C_{ijk\ell} = R_{ii'}R_{jj'}R_{kk'}R_{\ell\ell'}C_{i'j'k'\ell'}$, where $R_{nn'}$ are rotation matrices.

It is also possible for terms to appear. As an example, consider sound waves propagating in a moving fluid flowing along the x axis. In the laboratory frame, these can be described by the equation

$$\beta\partial_t^2 p = \rho_0^{-1}\nabla^2 p - 2\beta v_0\partial_x\partial_t p - \beta v_0^2\partial_x^2 p, \tag{4}$$

in which v_0 is the velocity of the unperturbed fluid in the laboratory frame. The term with mixed time and space derivatives $\partial_x\partial_t p$ associated with transport is known as a Willis coupling term when viewed through the lens of dynamic homogenization[14]. As we shall see in the sections on breaking inversion symmetry and on breaking reciprocity, this term results from the violation of both inversion symmetry and time-reversal invariance in the system. The $\partial_x^2 p$ term is the consequence of the anisotropy of the system; contrary to the Willis coupling, it could arise in a mirror-symmetric system.

Additional degrees of freedom in the medium

The continuum description of equations (1) and (2) focuses on the displacement field $\mathbf{u}(t,\mathbf{r})$. However, this may not be enough to encode all the relevant degrees of freedom in the system. As an example, mechanical degrees of freedom can be coupled with heat transport (in thermoelasticity) or with electromagnetism (in piezoelectricity and electrostriction[15]). Typically, the key feature of a piezoelectric crystal is the conversion of mechanical energy into electricity and back. As such, the electromagnetic field has to be included in the description of phononic materials when piezoelectric phenomena emerge. This example illustrates the interplay between symmetries and relevant degrees of freedom: inversion symmetry of bound charge distribution within the medium must be broken for piezoelectricity to occur and induce strain-dependent electric dipoles. When this is

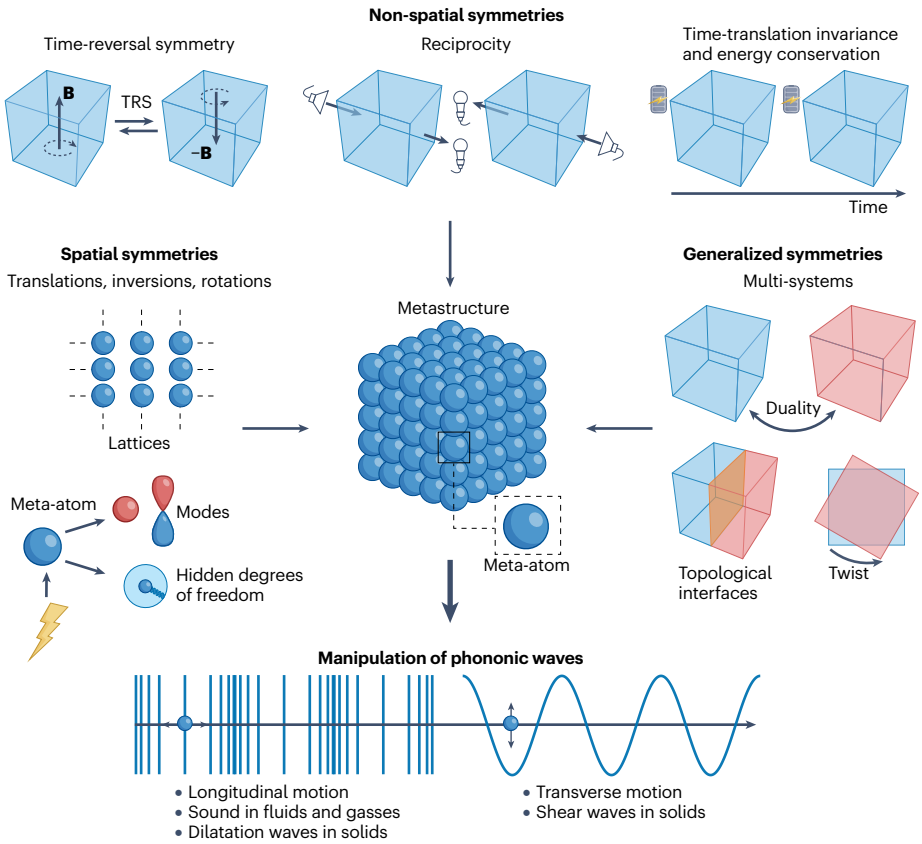

Fig. 1 | Symmetry-driven artificial phononic media. Schematics of the various symmetries characterizing phononic materials and metastructures, at both the microscopic and macroscopic scales. Breaking these symmetries enables enhanced control over acoustic and elastodynamic wave propagation. Symmetry classes include spatial and non-spatial symmetries, with the latter including reciprocity, time-reversal and time-translation invariance symmetry, and energy conservation, and the generalization of these symmetries to families of systems. TRS, time-reversal symmetry.

not the case, the mechanical and electrical degrees of freedom are decoupled and can be treated independently. Similarly, one must consider magnetoelastic effects in naturally occurring magnetic materials[16] and magnetoelastic metamaterials[17] via magnetic order parameters[18,19]. In the same vein, the polarization of acoustic waves requires consideration of the acoustic velocity field, not only of the scalar pressure field.

Besides this, additional mechanical degrees of freedom not captured by the instantaneous displacement field can play a role. In the simplest situations, these features can be captured by viscoelastic[20] or elastoplastic[21,22] models in which the deformation history affects the evolution of the deformation in a rate-dependent way, so the history of the displacement gradient $\nabla\mathbf{u}(t,\mathbf{r})$ must be included in the constitutive models. Alternatively, some aspects of microstructural deformation asymmetries may be retained in the constitutive description, as for micromorphic elasticity[23], of which micropolar (Cosserat) elasticity theories, which include microscale rotations and couple stresses, are a special case[23–28]. These can be necessary to describe metamaterials where complex unit cells lead to internal motions (known as non-affine deformations) that may deviate considerably from the (macroscopic) average. For instance, consider a half-filled bottle of water. If the bottle is not transparent, we cannot track the motion of the water, so the relationship between the total linear momentum and any directly observable displacement becomes non-trivial[29].

When the system is linear, several simplifications arise. In particular, we can perform a Fourier transform in space and time, which allows us to hide degrees of freedom at the price of having complex-valued 'non-local' material coefficients that depend on the wavevector $\mathbf{q}$ and the frequency ω and therefore represent a convolution in space and time. The convolution in time, in particular, represents a form of time-translation-invariant memory in the system. For instance, equation (3) becomes

$$\rho\omega^2 u_i(\boldsymbol{q},\omega) = C_{ijk\ell}(\boldsymbol{q},\omega) q_j q_\ell u_k(\boldsymbol{q},\omega). \tag{5}$$

The case of equation (3) would correspond to a constant $C_{ijk\ell}$ not depending on the wavevector $\mathbf{q}$ and the frequency ω. In fact, the material coefficients $C_{ijk\ell}(\omega)$ of conventional materials such as steel or air display a weak dependency on frequency owing to microscale behaviour such as molecular relaxation processes and internal friction[20,30]. From the perspective of rheology, this means that all materials have a viscous response in addition to an elastic response. In principle, this Fourier transform procedure allows us to eliminate many degrees of freedom, but keep in mind that we still need to keep track of the degrees of freedom we care about because we can experimentally manipulate or measure them, like the electric field in piezoelectricity. Equation (5) is deceptively simple: if we Fourier transform back to real time, the product of Fourier transforms becomes a convolution of the instantaneous strain and the relaxation function of the material[20], which makes the presence of memory explicit in the system. When the system is nonlinear, these simplifications do not hold, and a case-by-case approach is required. However, symmetries still constrain the possible nonlinear terms in the equations and can be harnessed to control the behaviour of the system[31,32].

Beyond continuum theories

In some situations, it may be necessary to describe the material as a collection of discrete units coupled to each other (for instance, a collection of masses connected by springs). This is the case, for instance, when an artificial material is physically constructed out of weakly coupled individual units such as resonators, whose size is not negligible when compared with the typical scale of spatial variations of the phononic wave propagating in the system. In some situations, a continuum description may also be insufficient even if we include many degrees of freedom[32,33].

In the context of wave propagation, the most common way of describing an assembly of coupled resonators or modes is temporal coupled-mode theory[34,35], whereby the evolution of the complex amplitude $a_n(t)$ of the resonant mode n is described by

$$\partial_t a_m = \sum_n L_{mn} a_n, \tag{6}$$

where the matrix (or operator) $\hat{L}$ with components L_{mn} represents the coupling between different modes (the operator $\hat{H} = \mathrm{i}\hat{L}$ is often called a Hamiltonian by formal analogy with quantum mechanics). In this case, the symmetry of the system arises from the interplay between the symmetry of the modes and of the geometry of their couplings, and is encoded in operators acting in the same space as $\hat{L}$. Analogously to atomic orbitals, as shown in Fig. 1, meta-atom modes can be scalar, vectorial (in which case a_n are the components of the modes) and so on. They can be further organized into a metamaterial with a crystalline structure, allowing one to design its symmetries on demand. In this coupled-mode theory, transformations of the degrees of freedom (that may or may not be symmetries) are encoded in invertible operators $\hat{U}$ acting in the same space as $\hat{L}$. The transformation $\hat{U}$ is a symmetry when it commutes with $\hat{L}$, that is, when $\hat{U}\hat{L} = \hat{L}\hat{U}$.

Getting a continuum theory from a mesoscopic description

The techniques to derive a continuum theory from a collective description of the individual elements of the material are known as coarse graining, averaging or homogenization[36]. In metamaterials described by linear equations of motion, homogenization can be achieved at the price of having frequency-dependent and momentum-dependent coefficients, which introduce non-localities into the homogenized description of the material. In the general case, however, approximations are required to remove irrelevant degrees of freedom by exploiting a separation of timescales using methods such as adiabatic elimination of averaging[37,38]. For instance, spatially periodic media, which are invariant under discrete spatial translations, can be treated using Bloch theory, whereas random media, which are on average translation invariant, can be described using disorder-averaging techniques. Correspondingly, the relation of the continuum fields to the microscopic degrees of freedom (which can be appropriately chosen combinations or disorder averages and so on) may change even though their physical meaning should always be the same. We refer to refs. 39–41 for more details including techniques and methods; to refs. 42–44 for interacting point particles; to refs. 45–47 for cases with less symmetry; to refs. 48–51 for Bloch–Floquet techniques for spatially periodic media; and to refs. 29,52,53 for ensemble average methods for disordered media.

Elastic solids: a case study

We now consider a generalization of equation (2) that describes the propagation of elastic waves in solids known as Willis materials[48], and that will serve as a case study throughout the Review.

The equation of motion of elastic waves in a solid takes the form

$$\partial_t \mu_i = \partial_j \sigma_{ij} + f_i, \tag{7}$$

in which μ_i is the density of linear momentum, σ_{ij} the stress tensor, and f_i the density of external body forces. In addition, we consider the constitutive relations

$$\begin{pmatrix} \boldsymbol{\sigma} \\ \boldsymbol{\mu} \end{pmatrix} = \begin{pmatrix} \mathbf{C} & \mathbf{S} \\ \tilde{\mathbf{S}} & \boldsymbol{\rho} \end{pmatrix} \begin{pmatrix} \nabla \mathbf{u} \\ \partial_t \mathbf{u} \end{pmatrix} \quad \text{or in index notation}$$
$$\sigma_{ij} = C_{ijk\ell}\partial_\ell u_k + S_{ijk}\partial_t u_k \tag{8}$$
$$\mu_i = \tilde{S}_{ik\ell}\partial_\ell u_k + \rho_{ij}\partial_t u_j$$

according to which the momentum density μ_i and the stress σ_{ij} are proportional to both the time and space derivatives of some displacement field $\mathbf{u}(t,\mathbf{r})$, which may or may not be the displacement of the centre of mass. This is in stark contrast with the behaviour of conventional solids discussed in the introduction, for which these constitutive relations are uncoupled.

In the constitutive relations in equation (7), the mass density $\boldsymbol{\rho}$ is no longer a scalar field, but a rank-two tensor that arises because the displacement field may not coincide with the displacement of the centre of mass, $\mathbf{C}$ is a rank-four elastic tensor, and the third-order tensors $\mathbf{S}$ and $\tilde{\mathbf{S}}$, known as Willis couplings[29,52,53], can be seen as the phononic analogue of bi-anisotropic tensors in electromagnetism[54–57], whose local version is rooted in spatial asymmetry. As discussed in the introduction, the quantities in equation (7) may be effective quantities that have to be properly defined on a case-by-case basis. In addition, all quantities in equation (7) may depend on the frequency ω and the wavevector $\mathbf{q}$ (for example, σ_{ij} is $\sigma_{ij}(\omega,\mathbf{q})$), making them non-local in space and time: the products in equation (7) represent a convolution in space and time. In this case, the material coefficients like $C_{ijk\ell}$ may be complex valued to encode phase lags between stress and strain at a material point. Typically, Willis coupling coefficients are connected to a weak form of non-locality[52,53] because the dynamic effective response of the medium depends on both the local response of the material point and its interaction with neighbouring heterogeneities, described by the gradients of the phononic fields. In the following, we define 'local' materials as those that are adequately described by linear response coefficients that do not depend on $\mathbf{q}$ (that is, in the $\mathbf{q} \to \mathbf{0}$ limit). This generally occurs if the microstructure of the medium is sufficiently small relative to the wavelength, leading the constitutive response at any material point to depend only on the fields at that point.

Breaking spatial symmetries

A bulk material, viewed from the continuum perspective, is invariant under all spatial translations, rotations and inversions. These are collectively known as isometries and form the Euclidean group $\mathbb{E}^d$ (where d is the dimension of space). These symmetries underpin constraints and conservation laws. For instance, translation and rotation symmetries lead to linear and angular momentum conservation, respectively[58], and point-group symmetries guarantee that quantities with different symmetries are decoupled[59–61]. This makes their selective breaking an efficient tool to engineer wave propagation within artificial media, which is the focus of this section.

Breaking translation symmetry

Inhomogeneities in a medium, such as a spatial interface between two materials, break spatial translation symmetries. In such a system, the

conservation of the physical momentum $\boldsymbol{\mu}$ that underlies the wave equations still holds, because it is related to the joint translation of the medium and the wave through Noether's theorem. In contrast, the translation of the waves alone is not a symmetry because the medium is inhomogeneous. As a consequence, another quantity called the wave momentum is no longer conserved[62–64]. Intuitively, this can be seen from the fact that at an interface, the refracted and reflected waves carry different wavevectors from the incident field. The spatial repetitions of such interfaces can result in band foldings or more complex structures, and scattering at single interfaces can be designed to manipulate waves in both the near and far fields. These aspects are the focus of this section.

Phononic crystals. In a phononic crystal[2], continuous translation invariance is broken, but the system remains invariant under a set of discrete translations collected in a group called a Bravais lattice[65]. This breaking of continuous translation invariance also partially breaks rotation and reflection symmetries: the remaining symmetries are captured in mathematical objects called space groups[59–61]. For instance, one could consider a version of equation (3) in which the elasticity tensor $\mathbf{C}(\mathbf{r})$ and the density $\rho(\mathbf{r})$ depend on the position $\mathbf{r}$ in a spatially periodic fashion, such as $\rho(\mathbf{r}) = \rho(\mathbf{r} + a\hat{\mathbf{e}})$, in which $a\hat{\mathbf{e}}$ is a vector defining the discrete periodicity of the phononic crystal.

To analyse such a system, we use Bloch–Floquet theory[59,65–67]. In a nutshell, the spatial periodicity $\mathbf{r} \to \mathbf{r} + a\hat{\mathbf{e}}$ implies that the plane waves $e^{i\mathbf{q}\cdot\mathbf{r}}$ and $e^{i(\mathbf{q}+\mathbf{G})\cdot\mathbf{r}}$, where $\mathbf{G}\cdot a\hat{\mathbf{e}} = 2\pi n$, $n \in \mathbb{Z}$, are indistinguishable, and so one can define the wavevector $\boldsymbol{q}$ on a reduced region called a Brillouin zone that has periodic boundary conditions. The wavevector space is therefore tiled with copies of a 'first' Brillouin zone centred around $\mathbf{q} = 0$. The resulting wave propagation is captured by a band structure, consisting of a set of dispersion relations $\omega_i(\mathbf{q})$ (and the corresponding vibrational modes) that are repeated periodically in the wavevector space outside the first Brillouin zone (the decomposition of vibrational modes on the different equivalent Brillouin zones describes how fast they spatially oscillate in various directions, which gives information on the behaviour of the system when an interface or a defect is present). This description encompasses and goes beyond the metamaterial picture, in which an effective continuum theory with modified material constants is used to describe the behaviour of the system probed at long wavelengths[2,41,68]. It can perturbatively be seen as the result of folding the dispersion relation of waves in a homogeneous medium into the first Brillouin zone, which can be further harnessed to control wave propagation by considering families of symmetries, as discussed in the section on generalized symmetries.

One of the key features of phononic crystals is that they can have bandgaps, that is, frequency bands where no wave propagation can occur. Mathematically, this can be understood using the 'transfer matrix' $\mathrm{T}(\omega, E, \rho)$, which describes the propagation of waves with frequency ω along a given direction through a finite region by relating the wave amplitudes on the left to those on the right[68–71]. For instance, the transfer matrix corresponding to the 1D version $\rho\partial_t^2 u = \partial_x \sigma$ with $\sigma = E\partial_x u$ is given by[72,73]

$$\begin{pmatrix} u_\mathrm{R} \\ \sigma_\mathrm{R} \end{pmatrix} = \mathrm{T}\begin{pmatrix} u_\mathrm{L} \\ \sigma_\mathrm{L} \end{pmatrix} \qquad \text{with} \qquad \mathrm{T} = \begin{pmatrix} \cos\vartheta & Z^{-1}\sin\vartheta \\ -Z\sin\vartheta & \cos\vartheta \end{pmatrix}, \tag{9}$$

in which L and R mean left and right, and where $Z = \rho c^2 \kappa$ is the impedance of the medium of dispersion relation $\omega = c\kappa$ with $c^2 = E/\rho$, and $\vartheta = \kappa h$. In a lossless medium, the eigenvalues of the transfer matrix are, in general, of the form $e^{\pm i q_\mathrm{B}}$, and the dispersion relation of the bands is given by $\mathrm{tr}\,[\mathrm{T}(\omega)] = 2\cos q_\mathrm{B}$, in which q_B is the (dimensionless) Bloch wavenumber, which is real valued for propagating (Bloch) states and purely imaginary for non-propagating states. (When u and σ have more than a single component, T is a larger matrix and these expressions have to be adjusted accordingly.) For the particular T in equation (9), we find that $q_\mathrm{B}(\omega) = \vartheta = \omega/ch$, so we recover the bulk dispersion relation. Consider now a phononic crystal obtained by alternating two media with different impedances $Z_{1,2} \equiv Z(1 \pm \epsilon)$, corresponding to a stepwise variation of $E(\mathbf{r})$ and/or $\rho(\mathbf{r})$. The transfer matrix corresponding to the unit cell is $\mathrm{T}_\mathrm{uc} = \mathrm{T}_1\mathrm{T}_2$ (T_i is obtained from T in equation (9) by replacing Z with Z_i). As $\mathrm{tr}\,[\mathrm{T}_\mathrm{uc}(\omega)]/2 = [\epsilon^2 - \cos(2\vartheta)]/(\epsilon^2 - 1)$, the inequality $|\,\mathrm{tr}\,\mathrm{T}| \leq 2$ does not always hold. When it does not, the Bloch wavenumber q_B is not real valued: the corresponding frequencies ω correspond to the bandgap in which waves cannot propagate. The critical frequencies ω^* at which solutions change from propagating (in the bands) to non-propagating (in the gap) are called band edges and correspond to exceptional points of the transfer matrix[74–77].

As a consequence, exceptional points can arise in the complex wavevector space even in passive lossless media. It is also possible to design them by exploiting the coexistence of multiple wave polarizations in planar elastodynamics. For instance, in elastic laminates with isotropic constituents, the polarization conversion between shear and dilatation waves can induce exceptional points even away from the edges of the Brillouin zone[78,79]. These conservative laminates can give rise to anomalous wave phenomena such as negative refraction[78] and beam steering[78,79]. By including an anisotropic component, it is also possible to break the symmetry of leftward and rightward waves and excite axially frozen modes with a finite transmittance despite a vanishing axial group velocity[80].

Going back to dispersion relations, it turns out that all the band structures of 1D layered systems are encapsulated in a compact universal manifold (Fig. 2a for the two-layer case discussed above), which depends only on the impedance mismatches (not on the volume fraction of the constituents nor on their specific physical properties) and from which it is possible to calculate the density of the gaps in the spectrum[81,82]. In Fig. 2a, the yellow part of the torus corresponds to gaps, its boundary to the band edges, and the band structure is constructed by wrapping a line (blue) around the torus.

The band folding approach can also be used at the subwavelength scale in the presence of locally resonant elements with a strong albedo close to resonance, as demonstrated by the structure-induced negative refraction of sound in crystalline metamaterials made of soda cans[83,84] (Fig. 2b). In parallel, the existence and size of bandgaps are also constrained by the symmetry of the system[85,86]. Overall, the domain of phononic crystals led to the development of various advanced mechanical properties including bandgaps for strong field confinement[87], waveguiding[88] and focusing[89]. Bandgaps have also been observed in internal gravity waves, a class of mechanical waves present in stratified fluids such as the oceans[90]. Besides, phononic crystals play a major role in the control of elastic polarizations, ranging from bandgaps with elastic polarization selectivity[91] to multiphysics interactions in cavity optomechanics where strong interactions between photons and phonons can be obtained in phoxonic structures acting as dual photonic–phononic crystals[92].

Broken translation invariance beyond phononic crystals. Phononic crystals (with their discrete translation invariance) are not the only way to produce structures that break translation symmetry while remaining uniform bulk materials in some sense. For instance, quasiperiodic,

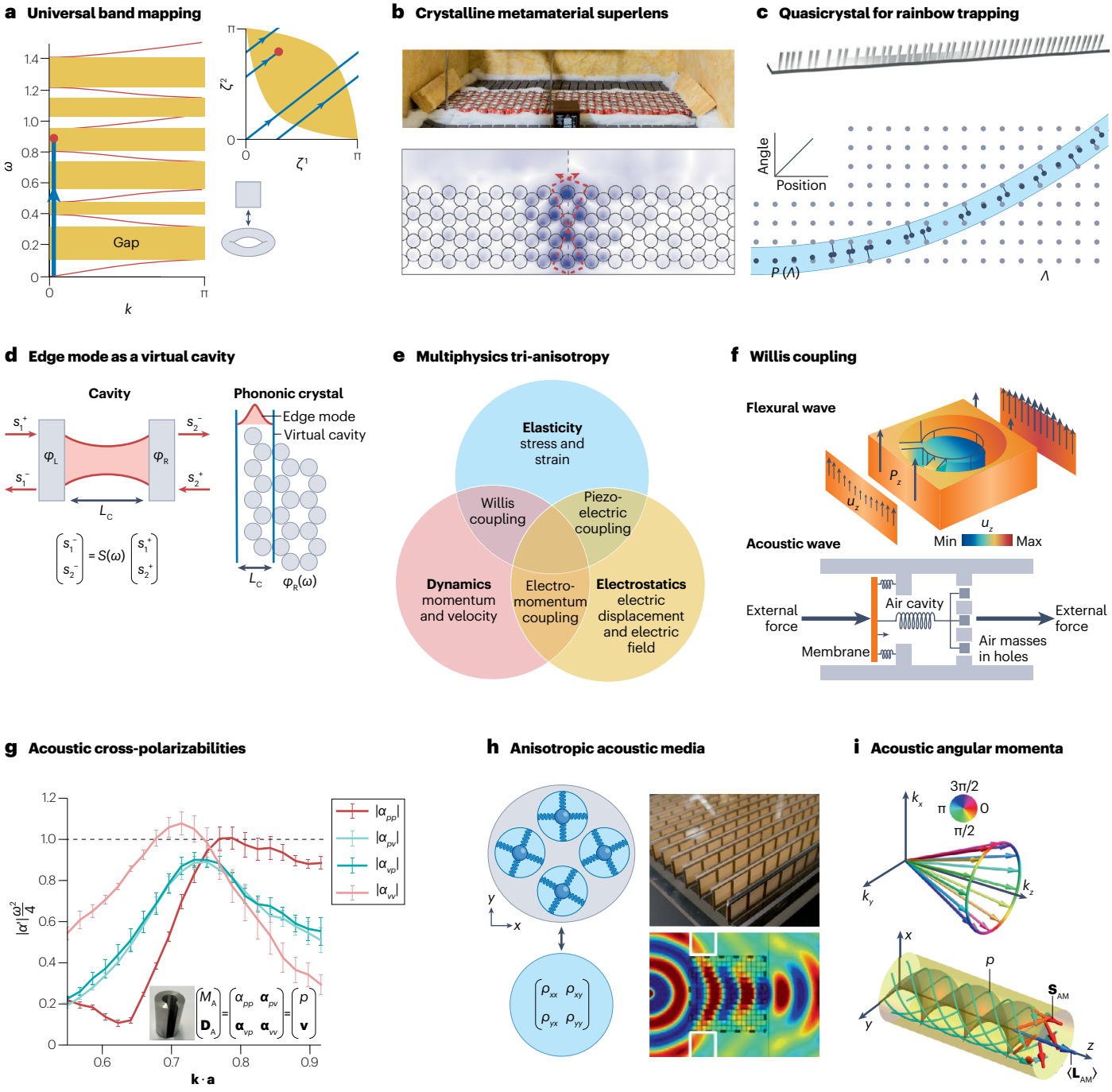

amorphous, hyperuniform or disordered systems can be seen as generalizations of phononic crystals. In these systems, slightly different approaches are required. Disordered and aperiodic systems cannot be handled using Bloch theory, as there is no translation invariance. However, these systems still have some regularity, which can be handled using non-commutative geometry, in which the Fourier space is replaced by a mathematical object called a C*-algebra[93–95]. This has been applied to phononic topological states[96–98] discussed in the next subsection. Quasicrystalline phononic structures, which can be seen as projections of higher-dimensional periodic structures in which the usual symmetry-based approach can be used, have also been extensively studied[99] for their bandgap properties[100], waveguiding[101,102], broadband asymmetric transmission[103], topological pumping[104,105] and fractal rainbow trapping[106] (Fig. 2c). In all these systems, non-local couplings can become important and affect wave propagation.

Engineering interfaces. The boundary of a medium is the most extreme case of spatial translation symmetry breaking. It is also an essential part in defining wave–matter interactions: the boundary permits interactions with the bulk. To engineer phononic devices,

Fig. 2 | Phononic phenomena induced by breaking spatial symmetries. **a**, Universal torus (obtained by connecting the opposite edges of a square, see inset) onto which all infinite band diagrams of 1D phononic crystals are mapped (main panel). The frequency ω acts as a time-like parameter defining a linear flow on the torus: $\vec{\zeta}(\omega) = \omega(h_1/c_1, h_2/c_2) \bmod \pi =: (\zeta^{(1)}, \zeta^{(2)})$, such that different crystals are mapped to flows of different slopes $\zeta^{(2)}/\zeta^{(1)}$; the gap region (yellow) is universal for crystals with the same impedance mismatch. **b**, Subwavelength-scaled crystal made of hollow soda cans for negative refraction and superlensing of acoustic surface waves (the dashed red lines show the corresponding ray tracing). **c**, Quasicrystalline phononic lattice (Λ) stemming from an effective projection onto a quadratic curve ($P(\Lambda)$) that is graded along its length, leading to fractal rainbow trapping. **d**, Correspondence between a conventional resonant cavity of length L_c made of two mirrors with reflection phases $\phi_{L,R}$ and described by a scattering matrix $S(\omega)$ (left) and a virtual cavity at the edge of a gapped phononic crystal, whose reflection phase $\phi_R(\omega)$ depends on the operating frequency, hosting a boundary mode. **e**, Multiphysics couplings in a tri-anisotropic medium: Willis coupling, piezoelectricity and electromomentum coupling. The local part of these interactions stems from different symmetry breakings at the subwavelength scale (Box 1). **f**, The application of a constant force F_z, equivalent to the total momentum along the z axis, P_z, on an asymmetrically structured beam results in strain $\partial_x u_z$, demonstrating non-zero Willis coupling for flexural waves (top). Schematic of an asymmetric scatterer responsible for airborne acoustic Willis coupling (bottom). **g**, Magnitude of the measured acoustic polarizability components within an asymmetric Helmholtz resonator (inset), normalized by the theoretical bound $4\omega^{-2}$. This shows maximal off-diagonal polarizabilities (α_{pv} and α_{vp} where p and v are the local pressure and velocity, respectively), which are scattering versions of acoustic Willis coupling, matching the conventional monopole and dipole polarizability. **h**, General model of an acoustic medium whose macroscopic effective response yields a dynamic mass density tensor (left). Acoustic metamaterial with membranes along one spatial direction, leading to hyperbolic wavefront propagation (right). **i**, An acoustic Bessel beam with a rotating phase profile in reciprocal space (top) is responsible for a vortex beam in real space (bottom) whose spiralling canonical momentum density p results in a non-zero integral orbital angular momentum $\langle \mathbf{L}_{AM} \rangle$. The local velocity polarization yields an additional spin angular momentum density $\mathbf{S}_{AM}$. Panel **b** adapted from ref. 84, CC BY 4.0. Panel **c** adapted with permission from ref. 106, American Physical Society. Panel **e** adapted with permission from ref. 138, Elsevier. Panel **f** (top) adapted from ref. 122, CC BY 4.0. Panel **f** (bottom) adapted from ref. 129, CC BY 4.0. Panel **g** adapted from ref. 123, Springer Nature Limited. Panel **h** (right) adapted with permission from ref. 153, American Physical Society. Panel **i** adapted with permission from ref. 162, American Physical Society.

we can either try to perform impedance matching to minimize the role of interfaces, or embrace them as an engineering knob. As an example, metasurfaces are 2D metamaterials that enable both control of surface waves in the near field and beam shaping in the far field through control of the structure and symmetries of the surface[5].

Another approach consists in harnessing boundary states that can exist at the interface between a medium and air, or between two media. The existence of such interface states can be captured from a scattering perspective[68–71], a description related to the transfer matrix approach mentioned above. When two good mirrors are placed face to face, they form a resonant cavity, where standing waves can be maintained until they are damped by losses, and whose resonant interaction with the environment is described by a scattering matrix $S(\omega)$ (Fig. 2d, left). These resonant modes are obtained by requiring that a round trip in the cavity leaves a wave in phase with itself. In other words, the dephasing $\Delta\phi$ picked during the round-trip should be a multiple of 2π. For a cavity of size L_c, $\Delta\phi = 2k(\omega)L_c + \phi_L + \phi_R$, where $k(\omega)$ is the dispersion relation of the medium in the cavity, and $\phi_{L/R}$ the reflection phases on the left/right sides. Now, let us consider a cavity where the walls are replaced with a phononic crystal. For frequencies ω in a bandgap, the phononic crystal acts as a frequency-dependent mirror with reflection phases $\phi_{L/R}(\omega)$ arising from the multiple interferences on the Bragg planes of the crystal. The solutions ω^* of $\Delta\phi(\omega) = 0$ [mod 2π] in the limit where $L_c = 0$ correspond to edge states (also known as Tamm states[107–109]). These edge states arise at the interface between the left and right phononic crystals, which act as a virtual cavity (Fig. 2d, right). This can be extended to cases where one of the media is vacuum or a boundary condition. In some instances, the presence of interface states can be traced to the existence of non-trivial topological invariants in the bulk[110–114]. Let us emphasize that this 'bulk–boundary correspondence' is not always valid[115–118], and that alternative approaches to define bulk topology suggest that the origin of certain non-symmetry-protected edge states may still be traced to the bulk[119,120].

Breaking inversion symmetry

Systems with inversion symmetry preserve the spatial symmetry or anti-symmetry of wavefield profiles, such as monopoles or dipoles. These can be related to different phononic physical quantities, making inversion-symmetry breaking a good design strategy for generalized bi-anisotropic and tri-anisotropic phononic media (Fig. 2e and Box 1). This is the focus of this subsection.

Willis coupling. As discussed, Willis coupling is described by the rank-three tensors in equation (7). If inversion symmetry ($\mathbf{r} \to -\mathbf{r}$) is present, the Willis coupling tensor $S_{ijk}(\omega,\mathbf{q})$ must satisfy $S_{ijk}(\omega,\mathbf{q}) = -S_{ijk}(\omega,-\mathbf{q})$ (the same is true for $\tilde{S}$). Hence, there is no Willis coupling in an inversion-symmetric local material (that is, for $S_{ijk}(\omega,\boldsymbol{q} \to 0)$). This can be understood from the fact that S_{ijk} relates a vector and a second-order tensor, which do not have the same symmetries. Conversely, purposely breaking the inversion symmetry of the elastic impedance[56,121,122] in metamaterials is a good design strategy to induce enhanced Willis couplings. As an example, the top panel of Fig. 2f shows the unit cell of an elastic structured beam made of resonant meta-atoms whose inversion symmetry is broken[122]. This directly results in a Willis coupling that relates the momentum (μ_z) and strain ($\partial_x u_z$) within the medium. In addition to the elastic case, breaking inversion symmetry also yields Willis couplings in the context of longitudinal sound propagating in fluids[51,56,123–128]. For instance, acoustic Willis couplings have been evidenced experimentally by using a subwavelength asymmetric scatterer in a 1D impedance tube measurement[129] (Fig. 2f, bottom).

We can gain insight on the microscopic origin of Willis coupling by sending a sound wave on a subwavelength scatterer (for which $ka \ll 1$, where a is the size of the scatterer and k the wavenumber). When the object is mirror symmetric, it scatters a monopole field M_A as a response to the local pressure p and a dipole field $\mathbf{D}_A$ as a response to the local velocity $\mathbf{v}$ field, which is captured by a polarizability tensor (inset of Fig. 2g). When the scatterer breaks mirror symmetry with respect to the direction of incidence, however, both the pressure and the velocity contribute to both the monopolar and the dipolar scattered fields. These cross-polarizabilities correspond to the scattering version of Willis couplings[124] and can lead to strong differences in the backward scattering from waves impinging from opposite directions[130]. The forward scattering remains the same as long as reciprocity holds. Breaking inversion symmetry within resonant scatterers can lead to

Box 1 | Breaking spatial symmetries

The elastodynamic and electrostatic response of a system is described by its constitutive relations that relate kinetic (stress **σ**, linear momentum **μ**, electric displacement **D**) and kinematic fields (displacement gradient $\nabla\mathbf{u}$, velocity $\partial_t\mathbf{u}$ and electric field $\mathbf{E}=-\nabla\phi$). It is possible to generate couplings between these equations by carefully breaking the relevant spatial symmetries. The system then becomes tri-anisotropic and can be described by a constitutive tensor whose off-diagonal constituents correspond to coupling quantities induced by symmetry breaking[142]. The 1D mass–spring model in the figure gives a simplified picture of the relation between spatial symmetry breaking and the associated off-diagonal terms; a more rigorous description can be found elsewhere[139]. Starting from the case of two identical masses linked by a spring, the application of symmetrical forces of equal amplitude on both sides of the system does not change the position of the centre of mass. If the masses are different, however, the centre of mass moves by $\Delta\mathbf{u}$, which differs from the displacement of the centroid. This results in the emergence of a non-zero linear momentum upon the application of a time-varying symmetrical stress **σ**, described by Willis coupling $\mathbf{S}\neq\mathbf{0}$. In addition, if the different masses have opposite electric charges, the time-varying symmetrical stress results in a non-zero global electric polarization $\Delta\mathbf{p}$. In turn, this yields an electric displacement field **D**, which is described by a piezoelectric coupling $\mathbf{B}\neq\mathbf{0}$. Building on this model of piezoelectric coupling, we can couple two identical dimers, asymmetric in charge and mass, in a mirrored configuration. This corresponds to spatial-inversion-symmetry breaking of the piezoelectric coupling itself, which can be modelled by a three mass–spring system with both mechanical and electrical spatially symmetric features, preventing the existence of global Willis $\mathbf{S}=\mathbf{0}$ and piezoelectric $\mathbf{B}=\mathbf{0}$ couplings. Nevertheless, the presence of an electric field **E** results in an asymmetric motion of the three charged masses driven by the Coulomb interaction $\mathbf{F}_q$, which changes the position of the centre of mass of the system. This leads to the emergence of electromomentum coupling, **W**, between the applied time-varying electric potential and the linear momentum. Finally, a global anisotropy of the medium — different responses as a function of the excitation direction — can be embedded into a dynamical mass density tensor. Although additional phenomena should be taken into account for the theoretical description of these couplings in a real material[142], this simplified mass–spring model highlights the origin of the dynamic effective field-coupling properties as spatial symmetry breaking at the microscopic scale.

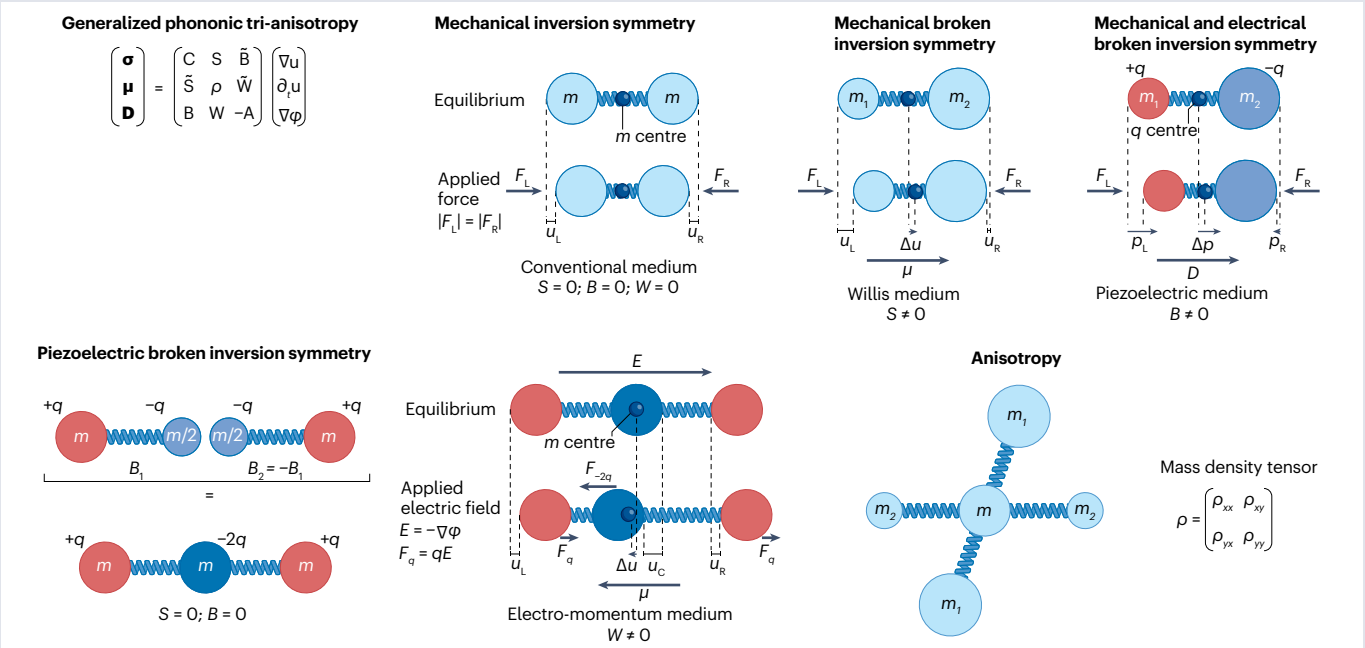

cross-polarizabilities of the same order as the diagonal ones[124], like in the split ring (Helmholtz resonator) in Fig. 2g. These can serve as building blocks for metamaterials showing strong macroscopic Willis couplings[56], whose asymmetric acoustic responses in reflection are relevant to wavefront shaping for sound[127,131–133] and elastic waves[122,134,135], as well as for particle manipulation[136].

Piezoelectricity and electromomentum coupling. Combined with the presence of electric charges, spatial inversion-symmetry breaking allows one to couple mechanical and electric fields. This electromechanical coupling is a feature of piezoelectric materials and is directly related to the broken centrosymmetry of their atomic structure[137]. It is evidenced by the change in electric polarization in the material upon mechanical strain. In turn, the inverse piezoelectric effect corresponds to the generation of stress in response to an electric field. Accordingly, the stress in a piezoelectric material is related to the gradient of the displacement field and the gradient of the electric potential field via the relation $\boldsymbol{\sigma}=\mathbf{C}:\nabla\mathbf{u}+\mathbf{B}^{\mathrm{T}}\cdot\nabla\phi$, where **B** is the piezoelectric coupling

tensor in stress-charge form and ϕ is the electric potential. Similarly, the electric displacement field $\mathbf{D}$ in a piezoelectric medium is a function of the same fields through the relation $\mathbf{D} = \mathbf{B} \cdot \nabla\mathbf{u} - \mathbf{A} \cdot \nabla\phi$, where $\mathbf{A}$ is the dielectric permittivity tensor.

Breaking inversion symmetry from the viewpoint of the piezoelectric properties of the medium leads to an emergent constitutive coupling between electrostatics and dynamics, as was first shown using source-driven continuum homogenization[138], and thereafter using retrieval methods[121] and discrete models[139]. In these systems, the electric polarization and velocity fields, as well as the linear momentum and the electric field, are coupled by the 'electromomentum' couplings[138] (Fig. 2e). As a result, each one of the kinetic fields (stress, linear momentum density, electric displacement) depends on all three kinematic fields (strain, velocity, electric field; Box 1), and therefore such materials are called tri-anisotropic materials. In symbolic matrix notation, the constitutive relations of electromomentum-coupled materials take the form

$$\begin{pmatrix} \boldsymbol{\sigma} \\ \boldsymbol{\mu} \\ \mathbf{D} \end{pmatrix} = \begin{pmatrix} \mathbf{C} & \mathbf{S} & \tilde{\mathbf{B}} \\ \tilde{\mathbf{S}} & \boldsymbol{\rho} & \tilde{\mathbf{W}} \\ \mathbf{B} & \mathbf{W} & -\mathbf{A} \end{pmatrix} \begin{pmatrix} \nabla\mathbf{u} \\ \partial_t\mathbf{u} \\ \nabla\phi \end{pmatrix}, \tag{10}$$

where $\tilde{\mathbf{W}}$ and $\mathbf{W}$ are the second-order electromomentum coupling tensors[140]. Like the Willis couplings[56] and the magnetoelectric couplings[141], the electromomentum couplings are required to ensure that the constitutive relations satisfy physical constraints[142]. Unlike Willis couplings, the electromomentum effect depends on the circuit conditions, yielding an intrinsic electrical tunability for wave manipulation[121,143,144] and scattering[145]. In addition, recent works analysing the polarizability of electromomentum-coupled scatterers[145,146] have shown that the polarizability tensor must consider both electric and magnetic field scattering owing to the time-varying nature of all fields, and that the polarizabilities coupling mechanical and electric fields can reach the same magnitude as the diagonal terms, even when the Willis coefficients vanish[121].

Breaking rotation symmetry

Breaking rotation symmetry permits us to engineer artificial media beyond isotropic constraints, providing tensorial richness to their mechanical response (Box 1). Rotational symmetry of the underlying medium also underpins the conservation of the angular momentum of the waves, which makes its breaking an efficient tool to control the chirality of phononic fields. These aspects are the focus of this subsection.

Anisotropy engineering. Isotropic materials are endowed with full rotation symmetry. In these systems, waves propagate in all directions in the same way (equations (1) and (2)). In contrast, anisotropic materials do not have full rotation invariance. When they are homogeneous, the remaining symmetries are contained in a mathematical object called a point group[59,60]. As a consequence of anisotropy, material properties must be encoded in (anisotropic) tensors, such as the elastic tensor $\mathbf{C}$ in equation (3). This has important implications for wave propagation[3,4,147]. As an example, consider a 2D collection of subwavelength resonators consisting of circular cavities carved in a rigid medium, which individually host a mass connected to the boundary by springs[29,148] (Fig. 2h, left). In such a system, the measurable displacement field does not necessarily coincide with the displacement of the centre of mass, because the internal masses may be hidden. Hence, the velocity $\mathbf{v}$ associated with the displacement field and the linear momentum density $\boldsymbol{\mu}$ are related through $\boldsymbol{\mu} = \rho\mathbf{v}$ through an effective mass density tensor of the form

$$\rho = \begin{pmatrix} \rho_{xx} & \rho_{xy} \\ \rho_{yx} & \rho_{yy} \end{pmatrix}, \tag{11}$$

whose components can be either positive or negative, corresponding to an in-phase or out-of-phase macroscopic response of the medium, respectively[29]. Acoustic waves in such a 2D anisotropic system can be described by a generalization of equation (1) in which[3] $\beta\partial_t^2 p = \partial_i([\rho^{-1}]_{ij}\partial_j p) = 0$, where ρ^{-1} is the matrix inverse of ρ. In a coordinate system where the mass density tensor is diagonal, the resulting dispersion relation is

$$\omega^2 = \frac{q_x^2}{\beta\,\rho_{xx}} + \frac{q_y^2}{\beta\,\rho_{yy}}. \tag{12}$$

This expression directly shows that the anisotropy affects the shape of the isofrequency contours of the system, which describe the spatial properties of wave propagation in the medium at the operating frequency ω in Fourier space. Indeed, depending on the relative signs of the eigenvalues of the mass density tensor, the isofrequency contours may have different topologies (open or closed), with fundamentally different consequences on wave behaviour[149]. As an example of open contour topology, phononic hyperbolic metamaterials support extremely anisotropic properties, such as broadband, diffraction-free directional ray-like propagation, negative refraction and enhanced wave–matter interaction[150–152]. These features have been evidenced experimentally for sound using membranes in a 2D waveguide[153] (Fig. 2h, right). Other acoustic implementations have been demonstrated in the context of hyperlenses[154,155], as well as in elastodynamics using patterned plates[156–159] and asymmetric pillars[160]. Following recent advances in nano-optics[151], sonic hyperbolic metasurfaces have also been proposed[161]. Rotation symmetry can be broken further in the case of multilayer phononic structures, leading to extremely anisotropic and reconfigurable wave propagation, as discussed in the section on twistronics.

Controlling the angular momentum of waves. In the same way that a phononic wavefield carries energy and linear momentum, it can also carry angular momentum $\mathbf{J} = \mathbf{L}_{AM} + \mathbf{S}_{AM}$, which can be decomposed into an orbital angular momentum $\mathbf{L}_{AM}$ and a spin angular momentum $\mathbf{S}_{AM}$ (ref. 13). The orbital angular momentum $\mathbf{L}_{AM} = \mathbf{r} \times \boldsymbol{\mu}$ is associated with rotations of spatial patterns in the wavefield and typically manifests as helicoidal wavefronts, as shown in the top panel of Fig. 2i in the case of an acoustic Bessel beam[162]. The spin angular momentum is associated with rotations of the polarization associated to the vector part of the wavefield. In acoustic waves, this means that one has to take into account the velocity field in addition to the scalar pressure field[13,163–165]. The corresponding spin density $\boldsymbol{S}_{AM} = \mathrm{Im}(\rho_0\mathbf{v}^* \times \mathbf{v})/2\omega$, where ρ_0 is the density of the fluid and $\mathbf{v}$ its velocity field, vanishes upon integration over the entire medium in homogeneous media, but it can be non-zero in the presence of field inhomogeneities[162,165] and for surface waves[166–168]. Hence, both elastic[169,170] and acoustic waves can carry a spin angular momentum (Fig. 2i, bottom).

Based on this, one can directly manipulate the angular momentum of phononic waves by engineering the breaking of rotation invariance of the propagating medium. For instance, it is possible to generate

$\mathbf{L}_{AM}$ in both acoustics and elastodynamics by using spiral-shaped tube sections[171,172] or with multiple sources with tailored phase delays[173]. One can also implement such rotation-symmetry breaking in the resonant structure of metasurfaces[174–179] to induce helicoidal wavefronts. Besides, the reduced planar rotation symmetry in some topological phononic crystals can be related to modes showing a local orbital angular momentum, which can induce vortices in the far field[180,181]. Breaking rotation invariance can also lead to spin–momentum locking, in which the direction of linear momentum determines the direction of $\mathbf{S}_{AM}$ (ref. 164), leading to spin-dependent propagation and selective wave routing at waveguide intersections[182].

A phononic spin–orbit coupling between orbital and spin angular momenta can also be induced by a mismatch between the rotation symmetries of the unit cell and the lattice. For instance, the elastic version of this behaviour has been obtained in microstructured mechanical materials[183,184] that twist in a specific direction when pushed along their axis, and proposed in quasicrystals[185]. In acoustics, spin–orbit coupling emerges in metastructures of dipolar modes with twisted intercell couplings, resulting in chirality-induced negative refraction[186]. These ideas have been applied in the context of imaging[187], multiplexing[188] and particle manipulation[189–192].

Breaking non-spatial symmetries

Usual phononic materials and their idealized versions show several non-spatial symmetries that are tightly connected to the specificities of the temporal dimension: reciprocity, time-reversal invariance, time-translation invariance and energy conservation. These symmetries, which are related to each other (Box 2), impose strong constraints on the behaviour of waves. Therefore, the combined breaking of spatial and non-spatial symmetries provides numerous opportunities for advanced phononic wave engineering, which is the focus of this section.

Breaking reciprocity

Spatial asymmetries can tailor the reflection and absorption of waves from opposite sides of a material, but are not sufficient to produce a genuine asymmetry in the transmission of waves between two points in space, like one would have in a diode[193]. As a wave propagates through a material, it undergoes a phase shift proportional to the distance travelled and an amplitude change due to the presence of losses. Usually, these modifications do not depend on whether the wave travels to the right or to the left, even in a inhomogeneous and arbitrarily shaped medium[130]. The reason for that is a discrete non-spatial symmetry known as reciprocity, which relates incoming and outgoing waves in a scattering process (Box 2). Non-reciprocal phononic media, where this symmetry is broken, can asymmetrically transmit mechanical energy, with potential applications in information and heat transport.

In practice, most ways of breaking reciprocity entail breaking spatial symmetries as well as time-reversal invariance ($t \to -t$), another fundamental discrete non-spatial symmetry that corresponds to reversing the flow of time, like watching the dynamics backwards. From the

Box 2 | Non-spatial symmetries from a scattering perspective

The scattering matrix S summarizes how waves are reflected and transmitted (scattered) off an object[68–71]. It has the same content as the transfer matrix, organized in a different fashion. Mathematically, it relates the amplitudes s_β^{in} and s_α^{out} or incoming and outgoing waves through different 'channels' (labelled by α, β...) through $s_\alpha^{out} = S_{\alpha\beta} s_\beta^{in}$.

The channels can be physical (waveguides) or abstract (different angles or polarizations).

In terms of the scattering matrix, the fundamental non-spatial symmetries that can be present in a phononic medium are[193,195,429] reciprocity $S = S^T$, energy conservation $SS^\dagger = 1$ and time-reversal invariance $SS^* = 1$. These symmetries are different from each other, so it is possible to have a medium response such as reciprocity without energy conservation (for example in a passive lossy medium). However, any two of the symmetries imply the third, so a lossless medium that is also invariant under time reversal must be reciprocal.

The scattering matrix associated to a set of resonant modes can be computed starting from coupled-mode theory. When the system is coupled with the outside environment (through the channels α), equation (6) becomes[34,35]

$$\dot{a}_m = L_{mn} a_n - \Gamma_{mn} a_n + W_{m\alpha} s_\alpha^{in} \quad \text{and} \quad s_\alpha^{out} = S_{\alpha\beta}^0 s_\beta^{in} + \tilde{W}_{\alpha n} a_n, \qquad (20)$$

in which the operator L describes the behaviour of the uncoupled system ($H = iL$ would be the Hamiltonian), Γ and W represent the loss and gain in the system due to exchanges of waves with the channels, respectively, $\tilde{W}$ represents the emission of waves in the channels from the resonant modes, and S^0 is the scattering matrix that the system would have if there were no resonant modes, that is, when $a = 0$. Probing the system with monochromatic waves at frequency ω eventually imposes $a(t) = Ae^{-i\omega t}$. Eliminating the resonant modes $a(t)$, we then find that the effective scattering matrix such that $s^{out} = S^{eff} s^{in}$ reads

$$S^{eff} = S^0 - \tilde{W}[L - \Gamma + i\omega]^{-1} W. \qquad (21)$$

This equation is known as the Mahaux–Weidenmüller formula[430]. In a system where energy is conserved, S^0 is unitary ($S^{0\dagger} S^0 = 1$), L is anti-Hermitian ($L = -L^\dagger$), and one must have $\partial_t \|a\|^2 = \|s^{in}\|^2 - \|s^{out}\|^2$, leading to a self-energy $\Gamma = 1/2 \tilde{W}^\dagger \tilde{W}$ and to $W = -\tilde{W}^\dagger S^0$. When in addition $S^0 = 1$, the Mahaux–Weidenmüller formula reduces to the more familiar form $S^{eff} = 1 + W^\dagger [L - \frac{1}{2} WW^\dagger + i\omega]^{-1} W$. In this framework, losses can be modelled by additional channels α with $s_\alpha^{in} = 0$ (on average), and for which one does not monitor the output s_α^{out}. Indeed, any purely dissipative (positive-semidefinite) loss term Γ can be modelled this way[431] by adding enough ports and setting $W \propto \Gamma^{1/2}$. From this scattering perspective, we reach three conclusions: engineering the coupling of a closed system to a radiation continuum is a way to induce effective non-Hermitian properties; the symmetries of L_0 and of the couplings directly influence those of S; and one can engineer poles and zeros of S, and even operate near them by exciting the system with complex frequencies. When the operator L depends explicitly on time, it is not possible to focus on a single frequency ω, and the above formalism has to be adjusted to account for the energy transfer to frequency harmonics. Note that the scattering matrix S and the coupling operators W and $\tilde{W}$ introduced in this box are different from and unrelated to the Willis and electromomentum coupling tensors $\mathbf{S}$, $\mathbf{W}$ and $\tilde{\mathbf{W}}$ in equation (10).

perspective of wave propagation, time-reversal invariance is related to the microscopic reversibility of the medium where waves propagate, which is violated by the presence of external biases such as magnetic fields or rotation. Yet in systems where energy is not conserved, it is in principle possible to have non-reciprocal systems that are time-reversal symmetric[194,195]. We refer the reader elsewhere[14,193,195–198] for more details on reciprocity in wave propagation.

Breaking reciprocity through an external bias. A common way of breaking reciprocity is to impose an external bias whose sign reverses under time-reversal symmetry, such as a magnetic field. Microscopic reversibility implies that the symmetry of the transmission coefficients is preserved only by reversing the bias when flipping the propagation direction. In contrast, holding the bias constant when interchanging source and receiver positions typically leads to a non-reciprocal response[199]. This works well in electromagnetism[197] because the propagation of light in certain materials is strongly influenced by available magnetic fields. It is also possible with phonons, for instance through magnetoacoustic couplings[200,201], but the effect is often weak. For instance, non-reciprocity induced by magnetoacoustic effects has been predicted and observed in surface acoustic waves[202,203], and can be strongly enhanced by the coupling with non-reciprocal spin waves[204–206]. Alternatively, one can use other external biases such as fluid flow[207–210], rotation[211] or odd/Hall viscosity.

In this context, the use of resonant components enables strong non-reciprocal effects with flow speeds much lower than the speed of sound. For example, a highly non-reciprocal acoustic circulator for audible sound was created using a ring cavity with a fluid spinning at a fraction of the speed of sound[212] (Fig. 3a). In the absence of an external bias, the two lowest-frequency modes in the circular cavity are degenerate with frequency ω_0. These correspond to clockwise and counterclockwise propagating waves, for which the pressure field takes the form $p_\pm(r,\phi) \sim e^{\pm i\phi}$ where ~ indicates proportional to, in polar coordinates, that can be combined into standing waves. When a background velocity field v is imposed (for example with fans), the frequencies of these modes undergo a Doppler shift $\Delta\omega_\pm/\omega_0 \sim \pm v/c$, leading to an acoustic Zeeman effect[212,213] that lifts the degeneracy. The resulting system can be captured by the coupled modes equation $\dot{a}_\pm = (i\omega_\pm - \gamma_\pm)a_\pm + W_{\pm,\alpha}s_\alpha^{in}$, in which $W_{\pm,\alpha} = \sqrt{2\gamma_\pm/3}\exp(\mp 2\pi/3(\alpha-1))$ represents the coupling to the three equispaced channels in Fig. 3a. Applying equation (21) gives the corresponding scattering matrix. In the simplified case where $\gamma_\pm = \gamma$ and the system is excited at $\omega = \omega_0$, we find that the transmissions between the channels 1 and 2 are

$$T_{1\rightleftarrows 2} = |S_{12/21}|^2 = \frac{4\gamma^2(\gamma \pm \sqrt{3}\,\Delta\omega)^2}{9(\gamma^2 + (\Delta\omega)^2)^2}, \tag{13}$$

from which we see that $T_{1\to 2} \neq T_{2\to 1}$ when $\Delta\omega \neq 0$, meaning that the system is not reciprocal, and that it is possible to tune $\Delta\omega$ to have $T_{1\to 2} = 0$.

This design was later used as a basis for theoretical and experimental investigations in topological acoustics in which the rings are put on a lattice[214–216], for non-reciprocal wave manipulation in the context of Janus metasurfaces[217] and to create non-reciprocal mode conversion in an elastic waveguide[218]. Alternatively, it is possible to have the fluid flow by itself, if it is made of self-propelled active components[112,219–221].

It is also possible to create non-reciprocal Willis couplings in spatially symmetric systems through external biases whose sign reverses under time-reversal symmetry. Going back to the example of Fig. 2g, the normalized cross-polarizabilities $\boldsymbol{\alpha}_{vp}$ and $\boldsymbol{\alpha}_{vp}$ relating the acoustic monopole $M_A = \alpha_{pp}p + \boldsymbol{\alpha}_{pv}v$ and dipole $\mathbf{D}_A = \alpha_{vv}\mathbf{v} + \boldsymbol{\alpha}_{vp}p$ to the pressure and velocities are also constrained by reciprocity, which imposes[124] $\boldsymbol{\alpha}_{vp} = -\boldsymbol{\alpha}_{pv}^T$. This constraint can be lifted by a constant bias[222], as in the spatially symmetric acoustic resonator embedded with a rotating flow in Fig. 3b. In a lossless system, this leads to $\tilde{\boldsymbol{\alpha}}_{vp} = \tilde{\boldsymbol{\alpha}}_{pv}^T$ (a situation referred to as a scattering version of odd Willis coupling in ref. 222), as showcased by the overlapping blue and red lines on the right panels of Fig. 3b. This results in a different power extinguished by the scatterer when excited from the left or from the right, in stark contrast with the reciprocal cross-polarizabilities obtained through inversion-symmetry breaking alone.

Breaking reciprocity by combining spatial asymmetries and nonlinearity. In nonlinear systems, it is possible to break reciprocity dynamically, without an external bias[223,224], for instance by combining spatial asymmetries with a medium whose properties depend on the amplitude of the wave. Putting a lossy material on one side of the nonlinear medium effectively makes the wave interact with a different medium when excited from either side, making the transmission direction-dependent, that is, non-reciprocal. This simple mechanism has been implemented and studied fundamentally[223,225–228], together with other nonlinear schemes based on related phenomena, such as phononic bandgaps[229,230], frequency conversion[231–233], self-demodulation[227,234], prestretched linkages[235] and hysteresis[236]. The combination of spatial asymmetry and nonlinearity is a common ingredient in all these schemes, as showcased by the non-reciprocal phononic wave transmission stemming from the intrinsic nonlinear acoustic radiation pressure at an interface between water and air[227] (Fig. 3c).

Non-reciprocal continuum phononic media. In the case of continuum media, reciprocity can be framed as a link between two different excitations and the corresponding responses. This constraint is known as Maxwell–Betti or Lorentz reciprocity. In the case study that we introduced at the beginning of the Review, it implies that[237]

$$C_{ijk\ell} = C_{k\ell ij} \qquad \tilde{S}_{ijk} = S_{jki} \qquad \rho_{ij} = \rho_{ji}. \tag{14}$$

For materials with electromomentum coupling, reciprocity further implies that $\tilde{W}_{ij} = W_{ij}$[142,238]. When the elastic tensor is real valued, breaking its major symmetry ($C_{ijk\ell} \neq C_{k\ell ij}$) also requires the violation of energy conservation. The same holds for the mass density tensor: active metamaterials with a non-reciprocal ρ_{ij} have been realized using feedback loops[239]. This is not the case for Willis coupling, for which the constraint due to energy conservation is different[126,237]. As we discussed, one of the simplest ways, mathematically, to obtain Willis coupling is to consider sound waves in a moving fluid, for which we obtain an energy-conserving non-reciprocal bi-anisotropic coupling[240]. Starting from the linearized conservation of mass ($\beta\partial_t p = -\partial_x v$) and of linear momentum ($\rho_0\partial_t v = -\partial_x p$), which combine into equation (1), and performing a Galilean boost ($\partial_t \to \partial_t - v_0\partial_x$) to account for the motion of the fluid at speed v_0, we end up with

$$\begin{pmatrix}\partial_x v\\ \partial_x p\end{pmatrix} = -\begin{pmatrix}\beta & \xi\\ \zeta & \rho_0\end{pmatrix}\begin{pmatrix}\partial_t p\\ \partial_t x\end{pmatrix} + \mathcal{O}(v_0^2), \tag{15}$$

where $\xi = \zeta = v_0\beta\rho_0 + \mathcal{O}(v_0^2)$ is cast as purely non-reciprocal acoustic Willis couplings. A similar feature occurs in colloidal solids driven by a flow[47,241,242]. Non-reciprocal Willis couplings have also been discussed

a Acoustic circulator based on a bias flow

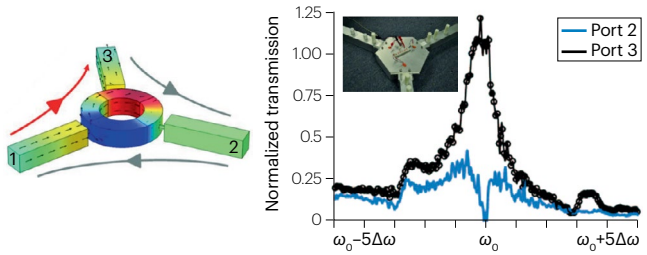

b Non-reciprocal Willis coupling based on a bias flow

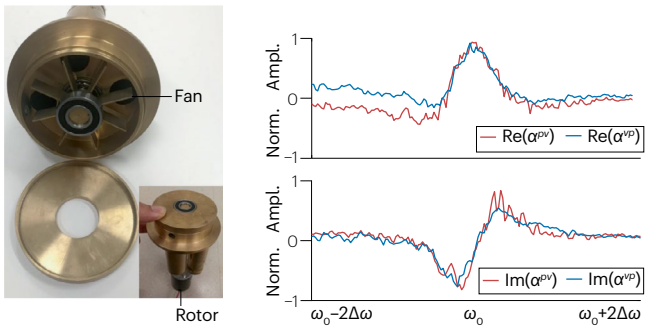

c Acoustic non-reciprocity from radiation pressure nonlinearity

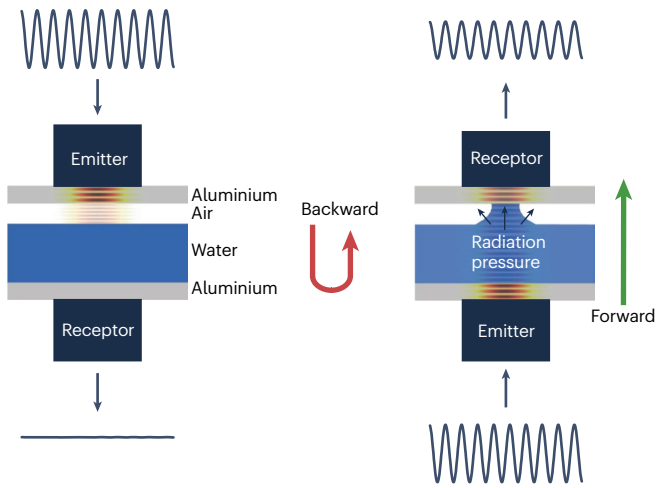

d Shock with transverse flow in a chiral fluid with odd viscosity

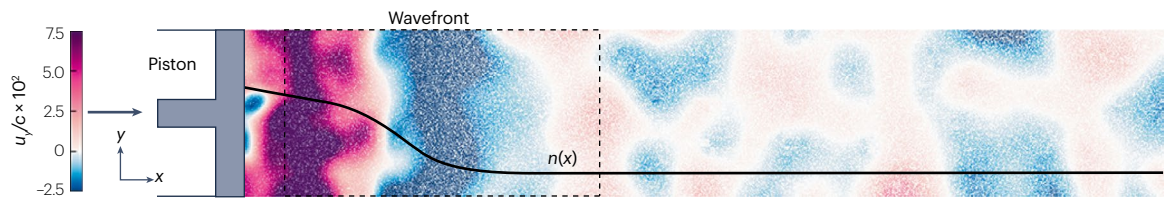

e Odd viscoelasticity in chiral biomaterials

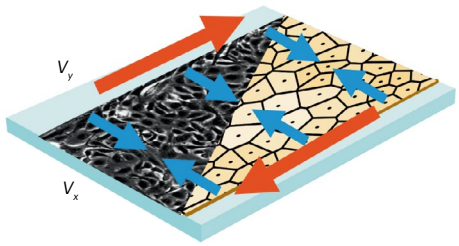

f Floquet topological insulator for sound

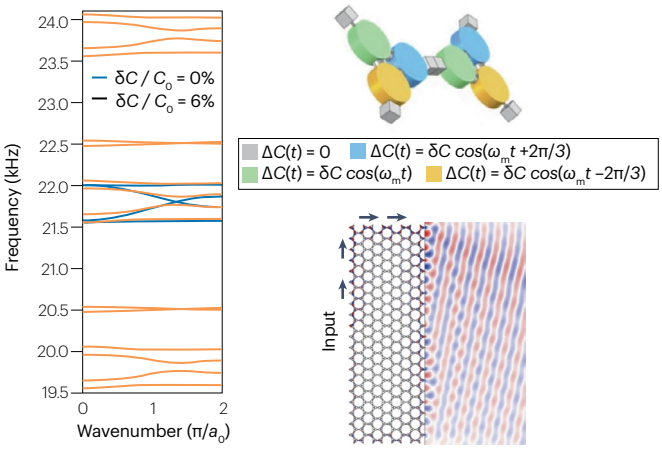

g Flexural wavepacket across a moving interface

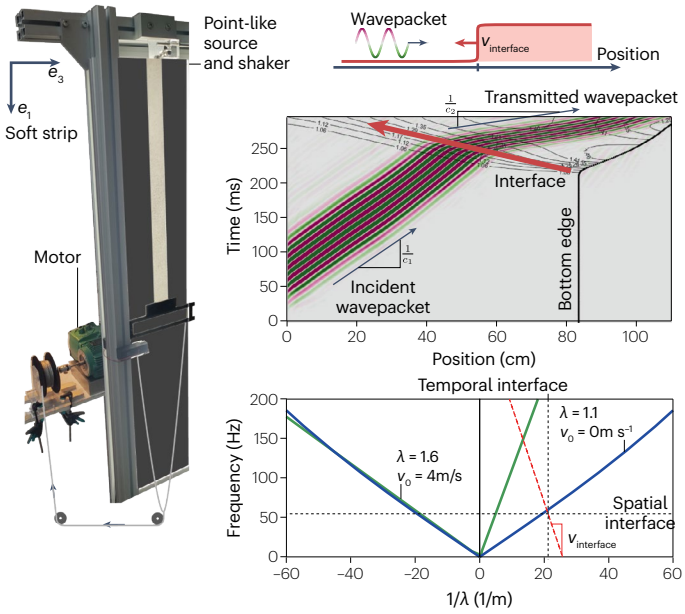

Fig. 3 | Phononic phenomena induced by breaking reciprocity, time-reversal and time-translation symmetry. a, An acoustic circulator based on a three-port cavity with embedded flow (left) at the resonance frequency produces zero transmission from port 1 to 2, and full transmission from port 1 to 3 (right). **b**, Experimental measurement of acoustic polarizations corresponding to odd Willis coupling induced by time-reversal symmetry breaking within a biased, spatially symmetrical scatterer. Here, the bias consists of an asymmetric flow, obtained with a motorized fan. **c**, Non-reciprocal ultrasonic transmission induced by the combination of spatial asymmetry and nonlinearity stemming from the acoustic radiation pressure at the interface between air and water: no signal is transmitted through the device in the backward configuration (left), while sound transmission mediated by radiation pressure in the fluid is permitted in the forward configuration (right) **d**, A shock wave propagating in a chiral fluid yields a directional transverse flow, as evidenced by the non-zero velocity u_y in the direction orthogonal to the shock (colour bar). **e**, Chiral biological tissues exhibit odd viscoelasticity, leading to transverse responses (red arrows) to constraints generated by cell proliferation and extrusion (blue arrows)[262]. **f**, Band structure of a Floquet topological insulator for sound (left) based on unit cells with a periodic time modulation of the acoustic capacitance $C = C_0 + \Delta C(t)$ at the frequency ω_m with a directional angular phase profile (top right), resulting in a topologically protected, non-reciprocal acoustic leaky-wave antenna (bottom right). **g**, Flexural wavepackets crossing a spatiotemporal interface upon the abrupt deformation of a soft elastomer (left). The experiment is carried out by abruptly stretching the medium using a motor while mechanical waves are launched in the medium (top right). This results in the non-conservation of both wavenumber and frequency between the impinging and refracted wavepackets, as shown in the real space–time diagram (middle right) and frequency–wavevector diagram (bottom right). This leads to different behaviour depending on the excitation direction. Panel **a** adapted with permission from ref. 212, AAAS. Panel **b** adapted from ref. 222, CC BY 4.0. Panel **c** adapted from ref. 227, CC BY 4.0. Panel **d** adapted from ref. 254, Springer Nature Limited. Panel **f** adapted from ref. 274, CC BY 4.0. Panel **g** adapted with permission from ref. 303, American Physical Society.

in passive systems such as moving fluids in zero-index metamaterials[240]. To induce strong non-reciprocal Willis effects going beyond the limitations imposed by passivity[243,244], active mechanisms such as electronic feedback loops[245,246], spatiotemporal modulation[247] and thermoacoustic amplifiers[248] have also been considered.

In (meta)fluids and viscoelastic media, non-reciprocal responses can also be encoded in viscosities that violate reciprocity, known as odd or Hall viscosities[249,250], corresponding to phonon Hall viscosities[251–253] in the context of phonons in solids. The Navier–Stokes equations take the general form

$$\rho(\partial_t + v_j\partial_j)v_i = -\partial_i p + \partial_j \sigma_{ij}, \tag{16}$$

where $\sigma_{ij} = \sigma_{ij}^{h} + \eta_{ijk\ell}\partial_\ell v_k$ is the stress tensor, split into a hydrostatic and a viscous part. The viscosity is encoded in a tensor $\eta_{ijk\ell}$, and reciprocity imposes that $\eta_{ijk\ell} = \eta_{k\ell ij}$. This constraint is, for instance, broken in chiral fluids made of actively spinning components and in magnetized polyatomic gases and plasma[250]. Consequences include non-reciprocal wave propagation[115,249,254–260], which can affect turbulence in the nonlinear regime[261] as well as topologically protected boundary modes[112,221,256] and nonlinear shock waves in compressible fluids[115,254,255] (Fig. 3d) and biological tissues[262] (Fig. 3e). These are typically manifested in transverse responses, for instance in the velocity field along the piston in a shock (colour in Fig. 3d) or edge flows (red arrows in Fig. 3e) that are a response to the flows towards the middle (blue arrows) due to the proliferation of cells in tissues.

Breaking time-translation invariance

Breaking time-translation invariance entails changing the physical properties of a system in time, so that wave excitations effectively see a different system or medium at different times. These time-dependent modulations require an active drive, which may inject or remove energy from the system. They can be designed to tune spatial and non-spatial symmetries of the system almost at will, at the price of a higher complexity and cost in design and operation compared with static systems. This approach permits one to adapt ideas related to the breaking of spatial translation invariance, although the specific nature of the temporal dimension and its ties to causality provide additional physical constraints that result in fundamentally different wave phenomena. In the case of periodic time modulations, time-translation invariance remains discrete, yielding the emergence of frequency harmonics. Single temporal interfaces result in different laws of refraction and reflection stemming from the conservation of momentum rather than frequency as in their spatial counterparts. These aspects of phononic time-varying media are reviewed in this section.

Time-periodic modulations. Although the time dependence can be arbitrary, theoretical and practical investigations have largely focused on periodic temporal modulations, because these are easier to handle. These driven systems are called Floquet systems[263–266], and sometimes 'time crystals'; we emphasize that this is a distinct concept from time crystals in statistical physics[267–270] and biology[271,272].

In Floquet systems, the dynamics are described by a periodically driven Hamiltonian $H(t)$ obeying $H(t) = H(t + nT_0)$ for any integer n, where T_0 is the modulation period. In contrast with time-independent systems, in which the linear response only occurs at the excitation frequency ω, periodically driven systems may show a response at harmonic components $\omega + n\omega_0$ ($n \in \mathbb{Z}$) spaced by $\omega_0 \equiv 2\pi/T_0$ (ref. 273), which are referred to as sidebands. Mathematically, the Floquet theorem[263] decomposes the evolution operator $U(t) = V(t)e^{itH_{eff}}$ associated with $H(t)$ into a T_0-periodic micromotion $V(t) = V(t + T_0)$ and a long-time evolution described by a time-independent effective Hamiltonian H_{eff}, called the Floquet Hamiltonian. For instance, Fig. 3f shows a tight-binding lattice of trimers of cavities whose acoustic capacitance is modulated in time[274], which shows sidebands as a repetition of the band structure along the frequency dimension. Floquet modulations can also result in wavenumber gaps, rather than frequency gaps as in their spatial counterparts. These host both amplified and damped modes that can exist because of the lack of energy conservation, as investigated in the context of spatial filtering[275].

It is possible to break time-reversal invariance in Floquet systems by choosing a $H(t)$ that is not an even function of time. (More precisely, we want to break time-reversal invariance $\Theta H(t)\Theta^{-1} = H(-t)$ in which Θ is the time-reversal operator. When a basis can be chosen so that $H(t)$ is real and Θ acts trivially, then this constraint reduces to $H(t) = H(-t)$, but this is not always true.) This is what happens in the modulated lattice of Fig. 3f, where the band degeneracies of the static medium are lifted upon dynamic modulation due to broken time-reversal symmetry induced by a spatially rotating phase profile[274]. This can induce non-reciprocal phonon effects with polarized coherent light[276]. A notable example is the phonon-mediated control of the magnetic properties of a lattice of spins to induce giant paramagnetism[277], phonon-driven magneto-valleytronics[278], or ferroelectricity[279]. Slower Floquet modulations that break time-reversal symmetry can effectively impart some

form of momentum and allow for strong non-reciprocal[280–287] or topological responses[274,288,289], or non-reciprocal acoustic devices such as robust leaky-wave antennas (Fig. 3f). It is also possible to emulate Floquet physics through the propagation of waves in static but spatially modulated media[290–292].

Time interfaces. Recent works have focused on the temporal analogues of spatial interfaces, which induce novel scattering wave phenomena that emerge when sudden, non-adiabatic changes occur to the properties of a medium without breaking spatial-translation invariance. For example, a temporal interface can be induced in a uniform medium in which the spatially uniform refractive index suddenly changes. Temporal reflections and transmission emerge at such temporal interfaces, with associated temporal Fresnel coefficients and a conservation of overall momentum instead of frequency and energy due to broken time-translation invariance but preserved spatial-translation symmetry[293,294]. Specifically, the incident wave is time reversed upon temporal reflection (negative frequency), in stark contrast with the conventional mirrored spatial reflection (negative wavevector). Various works have investigated these phenomena, both theoretically and experimentally, in 1D and 2D[295–298]. An example is the refocusing of water waves at the surface of a basin undergoing a rapid change in gravity[295], effectively behaving as an instantaneous version of a time-reversal mirror[299]. Soft elastomers[300,301], whose material properties depend on the medium deformation[302], are also a promising platform to implement spatiotemporal interfaces for phononic waves[303], in which a spatial interface travels at a finite velocity. The result of this interface breaking both spatial and temporal translation invariance are shown in Fig. 3g, demonstrating the non-reciprocal conversion of both wavenumber and frequency for a wavepacket impinging across the interface.

Breaking energy conservation

On a fundamental level, energy conservation is a consequence of time-translation invariance. In this section, we focus on systems where energy is not conserved, but that are effectively described by a time-independent equation. In this case, energy conservation means that some operators are Hermitian or anti-Hermitian. Consider the coupled-mode theory equation (6). If the energy E of the waves is proportional to $||a||^2 = \sum_m a_m^* a_m$ (where the star represents complex conjugation), then $\partial_t E \propto \partial_t \langle a, (L + L^\dagger) a \rangle$, in which $\langle \cdot, \cdot \rangle$ is a Hermitian inner product and † represents the conjugate transpose, and so energy is conserved when $L = -L^\dagger$, that is, when L is anti-Hermitian. In this case, the eigenvalues of L are purely imaginary and correspond to the frequency of oscillation of the modes. Equivalently, it means that the Hamiltonian $H = \mathrm{i}L$ is Hermitian. Conversely, systems with loss and gain are described by non-Hermitian (or non-anti-Hermitian) operators, leading to various properties common to these systems[304]. In this section, we discuss how a careful engineering of energy balance through gain and losses can be used to tailor wave propagation in lossy and active systems.

Balancing losses with gain in *PT*-symmetric systems. Systems in which the eigenvalues of the Hamiltonian H (the frequencies of oscillation) are purely real are called pseudo-Hermitian[304,305] or *PT*-symmetric. This includes lossless systems in which $H = H^\dagger$, but also systems where gain and loss are present but balanced. The label *PT* originally referred to the combination of parity P (space inversion) and time-reversal T, but it turns out that a more general class of systems shows the same mathematical properties[306,307], for which there is an anti-unitary operator PT with $(PT)^2 = 1$, such that $PTH = HPT$. In systems with (generalized) *PT*-symmetry, energy is not conserved in general, but when *PT*-symmetry is not spontaneously broken, it is effectively conserved when the system oscillates in a single eigenmode. A related symmetry known as anti-parity–time (*APT*) symmetry (in which $PTH = -HPT$) has also been considered to control heat transfer[308]. When $H = \mathrm{i}L$, H is *PT*-symmetric only if L is *APT*-symmetric, and conversely[309].

For example, consider a lossy resonator with complex eigenfrequency $\omega_0 + \mathrm{i}\gamma$ and couple it to an identical resonator with gain. We may aim at compensating the decay in the first resonator by choosing the amplification rate of the second one to be exactly equal to the loss rate of the first, that is, with intrinsic eigenfrequency $\omega_0 - \mathrm{i}\gamma$. If κ denotes the rate of energy coupling between them, the Hamiltonian becomes

$$H = \begin{pmatrix} \omega_0 + \mathrm{i}\gamma & \kappa \\ \kappa & \omega_0 - \mathrm{i}\gamma \end{pmatrix}. \tag{17}$$

The corresponding eigenvalues are $\omega_0 \pm \sqrt{\kappa^2 - \gamma^2}$, and the eigenvectors are proportional to $[\mathrm{i}\gamma \pm \sqrt{\kappa^2 - \gamma^2}, \kappa]^\mathrm{T}$. In the weak-coupling limit where κ is small, the system supports two distinct modes, with complex conjugate eigenvalues, close to those of the individual resonators. One mode is mostly localized in the gain resonator, and it grows in time, while the other decays in time at the same rate, as it mostly resides in the lossy resonator. An interesting phenomenon happens in the opposite regime of strong coupling, where $\kappa > \gamma$. When the energy has time to circulate back and forth between the resonators before decay or gain happens, gain and loss effectively compensate each other, and the eigenvalues of the system (although described by a non-Hermitian matrix) are purely real, that is, the modes do not grow or decay in time. This demonstrates the possibility of engineering non-Hermiticity and symmetries in a useful way, and the opportunities provided by *PT*-symmetry in the design of resonant phononic systems[310–312].

The eigenvectors of non-Hermitian matrices no longer necessarily form a complete basis, and are no longer orthogonal. Extreme cases occur where two eigenvectors become collinear and share the same eigenvalue, a situation known as an exceptional point[313–318]. This happens when $\kappa = \gamma$ in equation (17), for which H is not diagonalizable. The coalescence of the modes associated with the exceptional point has been evidenced in a two-level system consisting of two tightly coupled acoustic cavities with controllable asymmetric dissipation[314] (Fig. 4a). Moreover, the form and topology of the Riemann sheets formed by the eigensurfaces around an exceptional point has sparked various studies, such as the effect of dynamic encircling of exceptional points[316,319] to control the mode transmission, leading to optimized sound absorption[320], or the use of exceptional points for sensing[321,322].

Scattering in *PT*-symmetric systems. The scattering matrix S (Box 2) of a lossless system is unitary, and in the steady state the outgoing power is always equal to the incident power. Gains and losses affect this property and make the scattering matrix non-unitary. In particular, *PT*-symmetric systems can restore the flux conservation when operated under proper conditions (just like *PT*-symmetric cavities show no decay in the strong coupling limit when operated at a single eigenmode). In the case of scattering, *PT*-symmetric systems can support anisotropic transmission resonances[323], such that the system is totally transparent from one side, like a lossless system, but it strongly reflects from the opposite side. This response has been experimentally realized in a two-port acoustic system with active components[324] (Fig. 4b). Under this condition, gain does not simply compensate losses ($S_{12} = S_{21} = 1$), but it also cancels the reflection of the system from the lossy port ($S_{11} = 0$).

Excitation of the system from the opposite side yields strong reflections, despite the fact that full transmission is supported because of reciprocity, which is possible because energy conservation is broken by the presence of gain and loss. By extending this concept, it is possible to turn a complex disordered acoustic system, initially opaque, into a completely transparent one, by adding a distribution of gain and loss tailored to counteract the arbitrary impedance fluctuations initially present[325]. This results in a constant-pressure sound wave within an inhomogeneous sample consisting of a 1D array of active acoustic scatterers (Fig. 4c). Applications related to cloaking[326] and directional sound emitters[327] have also been explored.

Virtual gain or loss through complex frequency excitations. The presence of gain or loss in a medium implies the respective temporal growth or decay of the waves propagating in it. These aspects are associated with zeros and/or poles of the scattering matrix that are located outside of the real axis in the complex frequency plane, making them not reachable with a monochromatic excitation with purely real frequency. The usual way to circumvent this problem amounts to engineering the physical gain and loss in the system to move these poles and zeros towards the real frequency axis[328]. Alternatively, one can directly access the complex poles and zeros by exponentially increasing or decreasing in time the amplitude of waves used to probe the system. This effectively makes the operating frequency complex[329] and enables the excitation of scattering features beyond what is possible with a purely monochromatic signal on the real frequency axis. By doing so, it is possible to make passive systems effectively behave as if they had controllable gain or loss, without the inherent issues of stability and energy consumption associated with active protocols, which can make their practical realization challenging. First introduced in photonics[330–332], these concepts of virtual gain and loss have been applied to various non-Hermitian wave phenomena. For instance, virtual coherent absorption of elastodynamic waves has been achieved using counterpropagating signals exponentially growing in time, with a growth rate matching the leakage of the resonant inclusion[333,334]. Besides this, a temporally decaying signal has been used to implement the transient version of the non-Hermitian skin effect[335]. If applied to lossy superlenses, this virtual gain permits the dissipation in the system to be effectively compensated, enabling the recovery of their full subwavelength imaging potential, which is limited by non-local constraints[336] (Fig. 4d).

Amplification and nonlinearities. The presence of gain in a linear system eventually triggers nonlinearities that either stop growth or destroy the system. A typical example in wave physics is the appearance of a limit cycle, where the system starts oscillating by itself. This can be illustrated using coupled-mode theory (Box 2) by the equation

$$\dot{a} = \mathrm{i}\omega a - \gamma a + \left(\frac{\alpha^2}{\alpha + \beta|a|^2}\right)a \simeq \mathrm{i}\omega + (\alpha - \gamma)a - \beta|a|^2 a + \mathcal{O}(a^3) \qquad (18)$$

for a single complex mode $a(t)$. The second term represents saturable gain with amplitude α, which can be Taylor-expanded at small $|a|$ so we recognize the equation of a Stuart–Landau oscillator[37]: when $\alpha > \gamma$, the state $|a| = 0$ becomes linearly unstable and a limit cycle describing spontaneous oscillations of the form $a(t) = \sqrt{(\alpha-\gamma)/\beta}\,\mathrm{e}^{\mathrm{i}\omega t + \varphi_0}$ appears. This is the basis of the operation of a laser. Indeed, phonon lasers, the mechanical equivalent of light lasers, have been proposed and realized in several platforms[337–342]. Limit cycles, which can occur because of the presence of gain and loss, spontaneously break time-reversal symmetry (in addition to time-translation invariance). This can be harnessed to produce non-reciprocal scattering responses with reduced losses[343,344]. For instance, a sonic circulator based on spinning aeroacoustic limit cycles was realized[343] (Fig. 4e). An air flow orthogonal to the whistle cavity provides some gain that drives the system into a limit cycle whose sustained radiation synchronizes with the incident wave to compensate for absorption losses. More generally, nonlinear phononic media can exhibit a variety of phenomena related to underlying broken energy conservation and the possible spontaneous breaking of time translation, ranging from nonlinear travelling waves such as shocks and solitons to chaotic attractors[32,345,346].

Non-Hermitian skin effect. The non-Hermitian skin effect (NHSE) is a feature of certain non-Hermitian systems[304,347–349], in which eigenvalues and eigenmodes are highly sensitive to boundary conditions. Physically, it leads to the directional amplification or attenuation of waves within the medium and to field accumulation on some specific boundaries. In its simplest realization, the NHSE can be illustrated by a 1D chain of asymmetrically coupled resonators similar to the quantum Hatano–Nelson model[347,349]. In phononics, this can be captured by the coupled-mode equation

$$\partial_t a_n = \mathrm{i}[\omega a_n + \kappa_+ a_{n+1} + \kappa_- a_{n-1}], \qquad (19)$$

where integers n label the resonators, and where the amplitudes of the couplings $t_\pm$ to the left and to the right are different, mimicking a biased random walk. This effect has been related to the point gap topology of the corresponding non-Hermitian Hamiltonian[113]. In phononic media, the NHSE has been investigated in the presence of asymmetric couplings[350–355], odd elasticity[356,357] and odd mass densities[239]. Some designs use electronic feedback loops between microphones and speakers to obtain the NHSE for sound[353], as shown in Fig. 4f, which shows the accumulation of the acoustic signal at a single boundary, whatever the source position. The NHSE can also be observed in waves reflected by lossless topological systems, where it can lead to non-reciprocal Goos–Hänchen shifts[358].

Active continuum phononic media. As we discussed, the elastic tensor in equation (7) violates reciprocity when $C_{ijk\ell} \neq C_{k\ell ij}$. Similarly, energy conservation is violated whenever $C_{ijk\ell} \neq C^*_{k\ell ij}$ (ref. 237) (both constraints match when $\mathbf{C}$ is real valued). Such a situation, known as odd elasticity, can arise from the presence of non-conservative microscopic interactions[45,250] and has been realized with active elements[359,360], as in the example in Fig. 4g, showing a beam decorated with piezoelectric patches with designed feedback loops[359]. In such a metamaterial, quasistatic cycles between the bending and shear modes are associated with a non-zero amount of work whose sign depends on the cycle directionality. Such cycles could have implications for energy harvesting and sensing, and enable active wave propagation and instabilities within overdamped media[45,356,361] as well as adaptive locomotion of active solid metamaterials[360] (Fig. 4h). Conversely, the presence of these cycles means that it is impossible to have odd elasticity in a system where energy is conserved. Similarly, constraints on other material coefficients (such as ρ_{ij} and S_{ijk}) due to energy conservation[237] can be broken in media where energy is not conserved[222,239].

When $C_{ijk\ell}$ depends on frequency, it can also include a viscous part that dissipates energy, but can be passive. The combination of the two leads to a viscoelastic medium[20,30] in which $C_{ijk\ell}(\omega) = C_{ijk\ell}(0) + \mathrm{i}\omega\,\eta_{ijk\ell}(0) + \mathcal{O}(\omega^2)$, where $C_{ijk\ell}(0)$ and $\eta_{ijk\ell}(0)$ are the (zero-frequency) elastic and viscous tensors.

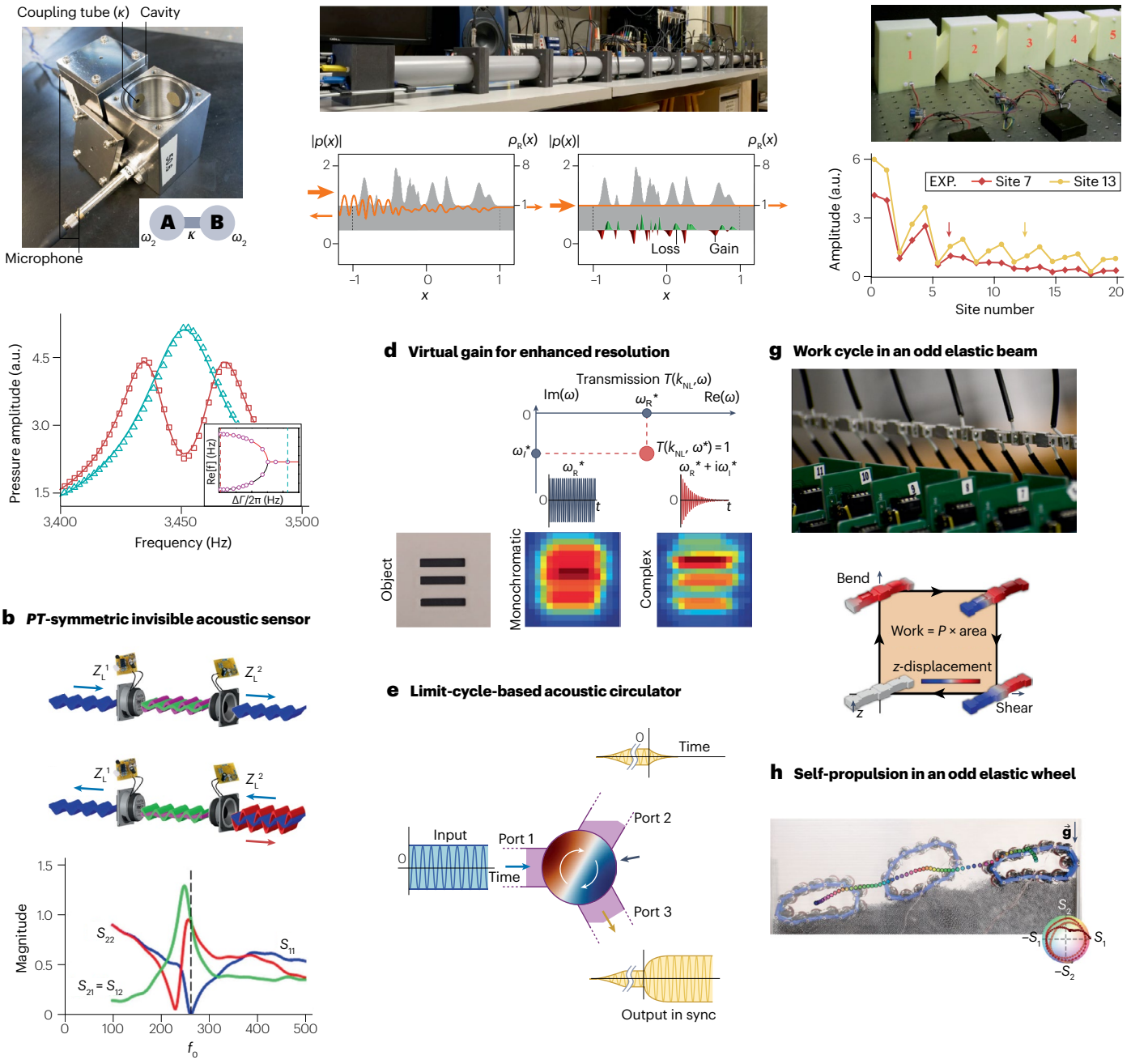

Generalized symmetries

In this section, we discuss several situations in which it is fruitful to consider the symmetries of multiple systems at once. We first discuss how the interface between two systems that have different symmetries (or different representations of the same symmetry) can host topological surface states. Then we discuss how generalizing symmetries to families of systems depending of parameters can allow us to identify additional hidden symmetries and to construct isospectral crystals. Next, we discuss how interpolating between different breakings of spatial-translation invariance can be used to enhance the control of the dispersion relation of phononic crystals. Finally, we discuss how in multilayer systems the symmetries of each layer can be harnessed to tailor wave propagation.

From symmetry to topology

Topological band theory is a framework that harnesses tools from topology to understand and control the behaviour of waves in materials, including their interfacial response. Symmetry plays a key role in the design of topological phononic crystals. In a nutshell, edge states often occur when the symmetry of states on both sides of an interface

Fig. 4 | Phononic phenomena induced by breaking energy conservation. **a**, A two-level non-Hermitian system made of two tightly coupled acoustic cavities with a coupling κ and controllable asymmetric loss Γ (top), which enables the demonstration of the coalescence of the two modes at the exceptional point (bottom, inset), evidenced by the merging of the two transmission peaks depending on the loss amount Γ. **b**, A unidirectionally invisible acoustic sensor at the design frequency f_0 based on *PT*-symmetry, showcasing unitary transmission ($S_{12} = S_{21} = 1$). The sensor is reflectionless from one side ($S_{11} = 0$) but has strong reflection from the other side (S_{22}, bottom, grey dashed line). Here, gain and loss are obtained with impedance circuit design through the use of different electrical loads Z_L in the two speakers. **c**, In a disordered Hermitian acoustic system, part of the incident signal is reflected owing to spatial variations of the medium properties (bottom left, grey area), but a tailored gain–loss distribution permits to obtain perfect transmission through the sample, along with no pressure variations within the system (bottom right). This non-Hermitian design has been implemented discretely using electrodynamic loudspeakers with a controlled acoustic impedance (top). **d**, The resolution of a conventional acoustic superlens is limited by its non-locality, which makes k_{NL} the largest accessible wavenumber, and by inherent dissipation, which pushes the corresponding unitary transmission $T(k_{NL},\omega^*) = 1$ below the real frequency axis (top). Using the associated complex excitation ($\omega^* = \omega_R{}^* + i\omega_I{}^*$), whose imaginary part is related to the losses of the system, instead of the monochromatic signal ($\omega_R{}^*$), results in a virtual gain that effectively compensates the losses in the lens and leads to enhanced resolution (bottom). **e**, A three-port nonlinear acoustic cavity hosts a limit cycle that continuously radiates a signal (yellow) through the ports; this signal synchronizes with the incident harmonic wave (blue), gaining energy from the limit cycle's emissions. In the presence of a bias, this enables loss-compensated non-reciprocal transmission. **f**, Non-Hermitian skin effect in a chain of active acoustic resonators based on asymmetric couplings, which are implemented using active feedback loops between speakers and microphones (top). The plot shows the directional field accumulation towards the left side of the chain, whatever the source position (bottom). **g**, Odd properties of the elastic response of a mechanical beam induced by using electrically controlled piezoelectric patches. In such a medium with an odd micropolar modulus *P* describing the asymmetric coupling between bending and shearing of the beam, a quasistatic cycle between bending and shear motion of the unit cell is associated with a non-zero work per unit volume whose sign depends on the direction of the cycle. **h**, Odd elastic mechanical systems can harness their work-generating cycles to produce emergent active functionalities, as illustrated by this adaptive wheel that displays uphill locomotion on a granular bed. Its propulsion is driven by odd couplings between two of its shear modes S_1 and S_2, whose shear-space trajectory is a noisy limit cycle (inset). Panel **a** adapted from ref. 314, CC BY 4.0. Panel **b** adapted from ref. 324, Springer Nature Limited. Panel **c** adapted from ref. 325, Springer Nature Limited. Panel **d** adapted from ref. 336, CC BY 4.0. Panel **e** adapted from ref. 343, CC BY-NC-ND 4.0. Panel **f** adapted from ref. 352, CC BY 4.0. Panel **g** adapted from ref. 359, CC BY 4.0. Panel **h** adapted from ref. 360, Springer Nature Limited.

does not match. More precisely, consider a system depending on a parameter p so that a band crossing occurs where two irreducible symmetric representations cross each other at some critical value p_c. At the interface between $p < p_c$ and $p > p_c$, a band crossing is susceptible to occur to interpolate between the band structures on both sides. In such a system, there is a bandgap on both sides of the interface (when $p \neq p_c$), but the gap closes at the interface. The existence of such an edge state is to some extent unavoidable and related to the topology of the band structure. This example illustrates a general principle that has been formalized in group-theoretical terms under the name of topological quantum chemistry[362,363], allowing a complete catalogue of topological phononic media to be obtained[364].

The lifting of band degeneracies through symmetry breaking is a common starting point for creating bandgaps and topological boundary modes. This is the case for Dirac cones in honeycomb lattices, singularities protected by time-reversal and inversion symmetries. Breaking time-reversal symmetry yields a Chern topological insulator exhibiting non-reciprocal phononic propagation at the edge that is robust against spatial disorder[214,215] (Fig. 5a). Breaking spatial-inversion symmetry while preserving time-reversal symmetry also opens a bandgap, leading to a valley-Hall insulator[365]. There, the edge modes between two mirrored lattices are only robust when a pseudo-spin associated to the two valleys is conserved. This emergent pseudo-spin can be harnessed to endow phononic waves with effective fermionic properties. This idea has been extensively investigated in phononics across multiple platforms such as lattices of pillars with different radii[366], which allow for pseudo-spins based on C_{6v} symmetry and dipolar and quadrupolar modes, whose conservation enables wave sorting (Fig. 5b). A similar symmetry-based strategy has been proposed to self-assemble topological phononic metamaterials[367].

Duality for phonons

The general definition of a symmetry, a transformation that leaves a system invariant, leaves room for other kinds of symmetries beyond the ones already discussed, which can be less straightforward, or somewhat hidden. As an example, two different configurations of a mass-spring chain (Fig. 5c) can share an identical band structure at the scale of the Brillouin zone, despite the absence of any conventional symmetrical relation between them. These 'hidden symmetries' may look accidental at first glance. To understand their nature, it is convenient to consider a family of systems continuously depending on a parameter p. Formally, to define a symmetry, the structure of the system needs to be encoded into a mathematical object such as the operator L introduced in the section on going beyond continuum theories, a Hamiltonian, or a dynamical matrix. Transformations are encoded into operators U, which are symmetries of L provided that $ULU^{-1} = L$. In this case, it is implicit that parameters are the same in $L = L(p)$ on both sides of the equation. Dualities can be seen as symmetries that also change the parameter p associated with the system: given a function $p \mapsto u(p)$, we say that U is a duality when $UL(p)U^{-1} = L(u(p))$. At fixed points p^* of u such that $u(p^*) = p^*$, known as self-dual points, the duality reduces to a conventional symmetry operation. The Onsager–Casimir reciprocal relations[14] relating the properties of systems with opposite external biases (such as magnetic fields) are an example of such a duality. The mechanical structure known as a twisted kagome lattice[368] provides an example with a more complex duality operator (Fig. 5d). In this case, the parameter $p = \theta$ is the twist angle, and H is the dynamical matrix of the phonons. The duality operator U shuffles the vibrational degrees of freedom in the unit cell, and $u(p) = -p$. Because of the duality within the family of twisted lattices, the band structures of dual systems are identical.

Other examples of mechanical systems dualities can be found elsewhere[369–371], including a systematic way to construct them[369]. In addition, the abstract Maxwell duality between floppy modes and states of self-stress[372–375] can also translate into a physical duality between parallelogram tilings and fibre networks[372]. Beyond the iso-spectrality of dual media, duality operations put additional constraints on the self-dual configuration, similarly to conventional symmetries. More generally,

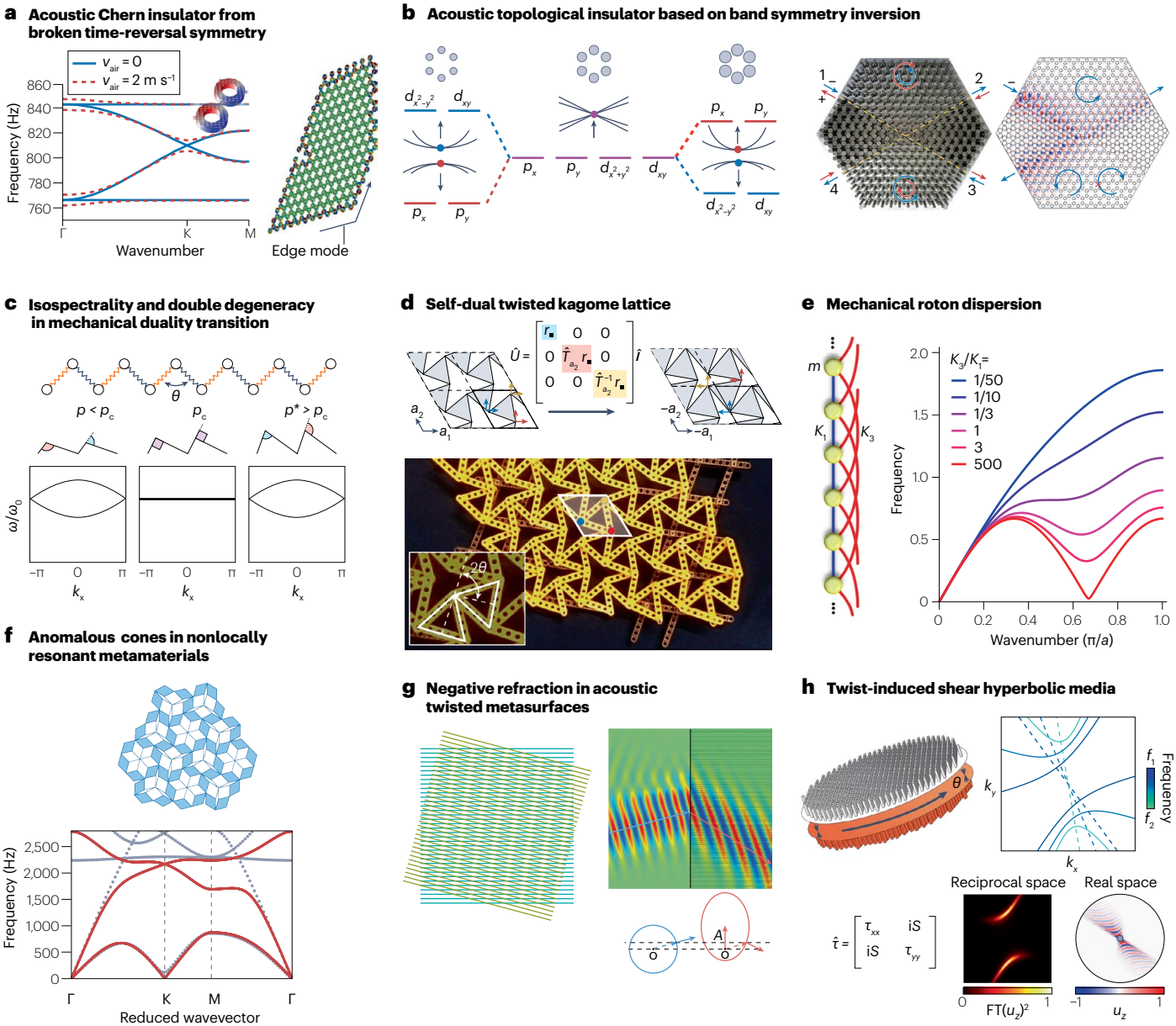

wave dualities have consequences for macroscopic elastic properties[46], and affect the propagation of waves at interfaces[376] as well as topological edge and corner states[377–379]. They also lead to pseudo-spin degeneracies unusual in mechanics that can be exploited to perform information processing using non-Abelian geometric phases[368].

Using families of symmetries to control phononic band structures

The crystallographic approach based on spatial symmetries is a powerful tool to engineer phononic crystals, but as the number of possible combinations of symmetries (space groups) is limited, this approach is not sufficient to finely control the shape of the bands. One way to circumvent this limitation is to use a parameter-dependent material to interpolate between different combinations of symmetries[380,381]. In particular, non-local metamaterials use couplings going beyond nearest-neighbours to control the propagation of waves[380,382–384]. Consider a monoperiodic chain of meta-atoms with families of couplings corresponding to different spatial ranges[380] (Fig. 5e). The systems with only blue couplings or only red couplings correspond to different discrete translation symmetries. While the periodicity of the system remains constant, the band curvature strongly depends on the ratio of the coupling strengths. This behaviour can also be seen as the result of the interaction of several chains of meta-atoms with different periodicities, which allows for multiple mode scales at a fixed frequency in the first Brillouin zone. In particular, the selective promotion of the third-order inter-cell couplings generates a dispersion relation with a local minimum that mimics the physics of rotons in superfluids. This roton-like dispersion has been experimentally implemented in 3D phononic metamaterials[380,385–389] and enables the propagation of multiple travelling waves with different wavenumbers and opposite

Fig. 5 | Generalized symmetries within families of phononic media. **a**, Flow-induced time-reversal symmetry breaking in an hexagonal acoustic lattice lifts the Dirac cone degeneracy and opens a topological bandgap described by a Chern invariant when the air velocity v_{air} in the lattice is non-zero. Such a phononic Chern insulator exhibits topologically protected non-reciprocal wave propagation at is boundaries. **b**, The preservation of C_{6v} spatial symmetry within triangular lattices of pillars, as well as the symmetrical band inversion induced by changing the radius of the pillars (left), results in helicoidal topological boundary states whose symmetry-engineered pseudo-spin (red indicates spin + and blue spin −) allows for wave sorting at topological crossings (right). The image on the left is a picture of the system, the one on the right is a simulation of the acoustic pressure field distribution. **c**, Three different configurations of a mass–spring chain show the emergence of a hidden symmetry, or duality, that results in two different lattices having the same band structure (left and right). At the self-dual point (centre), the duality becomes a symmetry of the medium and leads to a double degeneracy of the band for the entire Brillouin zone. **d**, In the plane, a twisted kagome lattice hosts a duality transformation U that rotates the displacements of the three masses (red, blue and yellow arrows in the schematic at the top) and translates them to different unit cells. This transformation is a combination of spatial and non-spatial transformations that goes beyond space group or internal symmetries. This non-trivial duality relates different twisted kagome lattices configurations (top left and right lattices), which can be implemented using Lego bricks (bottom picture) **e**, Changes in the dispersion relation for a 1D chain of masses and springs as a function of the ratio between first-order (K_1) and third-order couplings (K_3). For a ratio equal to 1, the dispersion is analogous to that of a roton. **f**, Zero-energy deformation mode within a non-locally resonant phononic metamaterial, which yields anomalous cones in the band structure emerging from zero frequency at the point K of the Brillouin zone, in contrast with the typical case of cones starting at the Γ point. **g**, A twist angle between two phononic crystal layers (left) induces negative refraction of acoustic waves (top right), described by a shift of the isofrequency contour in reciprocal space, which can be modelled by a spatially dependent gauge field A (bottom right). **h**, A twist angle between two detuned anisotropic elastic metasurfaces yields a hyperbolic effective material tensor $\boldsymbol{\tau}$ with non-Hermitian off-diagonal terms S (left). This leads to a frequency-dependent hyperbolic contour orientation of the bilayer (top right). This axial dispersion comes with an asymmetric distribution of losses, which results in shear hyperbolic wavefronts of the out-of-plane displacement u_z stemming from a point-source excitation, as shown in both reciprocal (Fourier transform (FT)) and real space (bottom right). Panel **a** adapted from ref. 214, CC BY 4.0. Panel **b** adapted from ref. 366, Springer Nature Limited. Panel **c** adapted from ref. 369, CC BY 4.0. Panel **d** adapted from ref. 368, Springer Nature Limited. Panel **e** adapted from ref. 380, CC BY 4.0. Panel **f** adapted with permission from ref. 381, American Physical Society. Panel **g** adapted with permission from ref. 399, AAAS. Panel **h** adapted from ref. 403, CC BY 4.0.

directions at the same frequency in a homogeneous material, as well as zero group velocity modes at the two inflection points. A similar strategy has been used to design delocalized zero-energy modes with a frequency $\omega = 0$ at a tunable wavevector $\mathbf{q} \neq \mathbf{0}$ by inducing non-trivial rigid motions within the medium using graph theoretical tools[381]. The hybridization of these modes with the waves propagating in the lattice generates anomalous cones in the dispersion relation emerging from arbitrary locations in the Brillouin zone (Fig. 5f) and leading to broadband negative refraction.

Twistronics for phonons

In multilayer systems, it is possible to combine the spatial symmetries associated with each layer, for instance by exploiting interlayer rotations. Recent works have started transposing the idea of twistronics[390] from electronic systems to phononics as an additional knob for wave control[391]. For example, the interplay between the spatial symmetries of the layers can generate superlattices controlled by the twist angle. The resulting moiré patterns, which have long-range periodicity at specific twist angles, are responsible for flat bands in the dispersion relation, which are tightly linked to field localization and strong resonant behaviour[392–396]. Moiré patterns can also emerge within a monolayer platform made of resonators whose positions are fixed but whose resonant properties are spatially modulated and rotated to introduce a structural mismatch with the underlying resonant lattice. Such twisted spatial modulations of a unique layer yield tunable wave behaviour, as demonstrated in hyperbolic phononic metasurfaces[160]. Beyond strictly periodic moiré patterns, twist-driven topological effects[397,398] and tunable gauge fields for negative refraction[399] relying on structural features (Fig. 5g) have been demonstrated over large angular ranges.

Beyond twist-induced lattice effects, interlayer rotations are relevant for anisotropic media, as showcased by twisted hyperbolic metasurfaces, where monolayers with hyperbolic dispersion are coupled and rotated with respect to each other[400–402]. By controlling the twist angle, the bilayer undergoes a topological transition between open and closed frequency contours for a broad range of frequencies, enabling broadband tunability of the directionality and localization of the wave propagation. In particular, the transition angle corresponds to a canalization regime with enhanced wave-matter interaction. Twist effects can also be used to rotate or shear dispersion relations in so-called twisted shear hyperbolic metasurfaces[403]. The corresponding orthogonality breaking between two detuned directional resonances makes it possible to control both the Hermitian and non-Hermitian features of the wave propagation. For a fixed twist angle, the principal axis of the hyperbolic medium rotates with frequency, and the spatial distribution of loss does not match the contour's symmetry. At the operating frequency, this translates into an effective material tensor $\boldsymbol{\tau}$, whose Hermitian part is diagonal while its non-Hermitian part presents some off-diagonal terms (Fig. 5h). Using the twist between two detuned hyperbolic metasurfaces, this effect can be maximized, and directly results in a screwed hyperbolic field profile where some branches are overdamped and others enhanced in comparison to a conventional hyperbolic medium. The combination of additional rotation-symmetry breakings within multilayer phononic media yields even more advanced wave manipulation[404], such as all-angle directional canalization of sound[405].

Outlook

As showcased throughout this Review, a symmetry-driven approach is a successful paradigm for the advanced manipulation of phononic fields across a wide range of domains and scales. In systems where energy conservation is broken, a frontier consists in engineering active and time-dependent media with feedback, in which wave propagation can be controlled at will through feedback loops. The future development of multiphysics concepts such as electromomentum or magnetomomentum couplings has great potential to push the levels of reconfigurability of phononic media beyond what is currently possible. In particular, the ability to implement extremely fast modulations of the global properties of the medium over a large scale would allow the investigation of out-of-equilibrium physical phenomena[406] and the use of time as an extra tuning parameter in the context of 4D metamaterials[407]. Reconfigurable acoustic metasurfaces paired with optimization protocols have also proven to be a crucial tool for wavefield shaping, allowing advanced multiplexing of acoustic communication in complex

environments[408]. Alternatively, the use of active matter[112,409] or flexible soft elastomers[300–302] to modify the properties of the propagating medium opens the door to complex dynamic wave phenomena with analogies with the behaviour of active solids ranging from biological tissues to soft robotic materials[112,250,360,409–413]. Focusing on the zero-frequency response of the medium[31,414], active components open avenues for autonomous metamaterial-based machines relevant for sensing, shape-morphing and object manipulation. Conversely, the use of activity often requires taking into account instabilities and nonlinearities, which can be used to create new functionalities. In this context, new ideas and implementations linked to non-Abelian, non-Hermitian and nonlinear topological phenomena, as well as topological defects and disordered topological phases, have emerged as a means to control acoustic and optical fields[415–417]. These directions hold promise for next-generation computation and telecommunications applications built on topologically robust devices.

The symmetry-driven approach described in this Review goes beyond artificial media and also applies to natural materials. In the near-infrared optical frequencies, the vibrations of atomic lattices (phonons) can interact with light to create quasiparticles called phonon-polaritons, whose symmetry-related properties, such as hyperbolicity, are currently under extensive study[418]. Controlling the propagation of these hybrid surface waves, either via twisted multilayer systems or artificial patterning, is at the heart of modern nanophotonics, and future investigations combining both spatial and time symmetries, such as Floquet polaritonics, are promising research directions. Beyond phonon-polaritons, it has been recently demonstrated that phonons in natural alpha-quartz show intrinsic chirality[419]. Phonons are also related to heat transport[420], and the symmetry-based approach also applies to this diffusive regime, as showcased by thermal systems with anti-parity–time symmetry[308] and twisted thermal metasurfaces[421].

Going beyond standard symmetries, the examples of generalized symmetries we discussed, such as twist symmetries or dualities, show that the symmetry-based approach discussed in this Review is open-ended, as new kinds of symmetries can emerge. Finally, symmetry-based approaches can complement the inverse design methods and machine-learning techniques that have been developed in the past decade to design artificial metastructures[422–427], for instance in equivariant machine-learning techniques[428].

Published online: 15 December 2025

References

1. Curie, P. Sur la symétrie dans les phénomènes physiques, symétrie d'un champ électrique et d'un champ magnétique. *J. Phys. Theor. Appl.* **3**, 393–415 (1894).
2. Deymier, P. A. *Acoustic Metamaterials and Phononic Crystals* Vol. 173 (Springer, 2013).
3. Ma, G. & Sheng, P. Acoustic metamaterials: from local resonances to broad horizons. *Sci. Adv.* **2**, e1501595 (2016).
4. Cummer, S. A., Christensen, J. & Alù, A. Controlling sound with acoustic metamaterials. *Nat. Rev. Mater.* **1**, 16001 (2016).
5. Assouar, B. et al. Acoustic metasurfaces. *Nat. Rev. Mater.* **3**, 460–472 (2018).
6. Craster, R. V., Guenneau, S. R., Muamer, K. & Wegener, M. Mechanical metamaterials. *Rep. Prog. Phys.* **86**, 094501 (2023).
7. Truesdell, C. & Toupin, R. in *Principles of Classical Mechanics and Field Theory* (ed. Flügge, S.) 226–858 (Springer, 1960).
8. Truesdell, C. & Noll, W. *The Non-linear Field Theories of Mechanics* (Springer, 2004).
9. Landau, L. & Lifshitz, E. *Fluid Mechanics* 2nd edn (Butterworth-Heinemann, 1987).
10. Landau, L., Landau, L., Lifshitz, E., Kosevich, A. & Pitaevskii, L. *Theory of Elasticity* 3rd edn (Butterworth-Heinemann, 1986).
11. Pierce, A. D. *Acoustics* 3rd edn (Springer, 2019).
12. Achenbach, J. D. *Wave Propagation in Elastic Solids* (Elsevier, 1973).
13. Bliokh, K. Y. Momentum, spin, and orbital angular momentum of electromagnetic, acoustic, and water waves. *Contemp. Phys.* **65**, 219–238 (2025).
14. Nassar, H. et al. Nonreciprocity in acoustic and elastic materials. *Nat. Rev. Mater.* **5**, 667–685 (2020).
15. Gerhard, R. in *Electromechanically Active Polymers* (ed. Carpi, F.), 489–507 (Springer, 2016).
16. Lee, E. W. Magnetostriction and magnetomechanical effects. *Rep. Prog. Phys.* **18**, 184–229 (1955).
17. Lapine, M., Shadrivov, I. V., Powell, D. A. & Kivshar, Y. S. Magnetoelastic metamaterials. *Nat. Mater.* **11**, 30–33 (2011).
18. Reid, A. H. et al. Beyond a phenomenological description of magnetostriction. *Nat. Commun.* **9**, 388 (2018).
19. Trémolet de Lacheisserie, E., Gignoux, D. & Schlenker, M. *Magnetism* (Springer, 2005).
20. Lakes, R. S. *Viscoelastic Materials* (Cambridge Univ. Press, 2009).
21. Liu, W., Janbaz, S., Dykstra, D., Ennis, B. & Coulais, C. Harnessing plasticity in sequential metamaterials for ideal shock absorption. *Nature* **634**, 842–847 (2024).
22. Wallen, S. P., DeLima, W. & Haberman, M. R. Strongly nonlinear wave propagation in elasto-plastic metamaterials: low-order dynamic modeling. *J. Mech. Phys. Solids* **204**, 106276 (2025).
23. Maugin, G. A. & Metrikine, A. V. *Mechanics of Generalized Continua* (Springer, 2010).
24. Cosserat, E. M. P. & Cosserat, F. *Théorie des corps déformables* (Hermann et fils, 1909).
25. Mühlhaus, H. (ed.) *Continuum Models for Materials with Microstructure* (Wiley, 1995).
26. Toupin, R. A. Elastic materials with couple-stresses. *Arch. Ration. Mech. Anal.* **11**, 385–414 (1962).
27. Mindlin, R. D. Micro-structure in linear elasticity. *Arch. Ration. Mech. Anal.* **16**, 51–78 (1964).
28. Ehlers, W. & Bidier, S. Cosserat media In *Encyclopedia of Continuum Mechanics* 436–446 (Springer, 2020).
29. Milton, G. W. & Willis, J. R. On modifications of Newton's second law and linear continuum elastodynamics. *Proc. R. Soc. Lond. A* **463**, 855–880 (2007).
30. Lakes, R. S. *Viscoelastic Solids* (CRC, 1998).
31. Bertoldi, K., Vitelli, V., Christensen, J. & van Hecke, M. Flexible mechanical metamaterials. *Nat. Rev. Mater.* **2**, 17066 (2017).
32. Lapine, M., Shadrivov, I. V. & Kivshar, Y. S. Colloquium: nonlinear metamaterials. *Rev. Mod. Phys.* **86**, 1093–1123 (2014).
33. Kevrekidis, P. G., Kevrekidis, I. G., Bishop, A. R. & Titi, E. S. Continuum approach to discreteness. *Phys. Rev. E* **65**, 046613 (2002).
34. Fan, S., Suh, W. & Joannopoulos, J. D. Temporal coupled-mode theory for the Fano resonance in optical resonators. *J. Opt. Soc. Am. A* **20**, 569 (2003).
35. Suh, W., Wang, Z. & Fan, S. Temporal coupled-mode theory and the presence of non-orthogonal modes in lossless multimode cavities. *IEEE J. Quantum Elect.* **40**, 1511–1518 (2004).
36. Pavliotis, G. A. & Stuart, A. M. *Multiscale Methods: Averaging and Homogenization* (Springer, 2008).
37. Kuramoto, Y. *Chemical Oscillations, Waves, and Turbulence* (Springer, 1984).
38. Kunihiro, T., Kikuchi, Y. & Tsumura, K. *Geometrical Formulation of Renormalization-Group Method as an Asymptotic Analysis: With Applications to Derivation of Causal Fluid Dynamics* (Springer, 2022).
39. Willis, J. R. Effective constitutive relations for waves in composites and metamaterials. *Proc. R. Soc. Lond. A* **467**, 1865–1879 (2011).
40. Craster, R. & Guenneau, S. *Acoustic Metamaterials: Absorption, Cloaking, Imaging, Time-Modulated Media, and Topological Crystals* Vol. 345 (Springer Nature, 2024).
41. Srivastava, A. Elastic metamaterials and dynamic homogenization: a review. *Int. J. Smart Nano Mater.* **6**, 41–60 (2015).
42. Born, M. & Huang, K. *Dynamical Theory of Crystal Lattices* (Clarendon, 1956).
43. Lutsko, J. F. Generalized expressions for the calculation of elastic constants by computer simulation. *J. Appl. Phys.* **65**, 2991–2997 (1989).
44. Irving, J. H. & Kirkwood, J. G. The statistical mechanical theory of transport processes. IV. The equations of hydrodynamics. *J. Chem. Phys.* **18**, 817–829 (1950).
45. Scheibner, C. et al. Odd elasticity. *Nat. Phys.* **16**, 475–480 (2020).
46. Fruchart, M. & Vitelli, V. Symmetries and dualities in the theory of elasticity. *Phys. Rev. Lett.* **124**, 248001 (2020).
47. Poncet, A. & Bartolo, D. When soft crystals defy Newton's third law: nonreciprocal mechanics and dislocation motility. *Phys. Rev. Lett.* **128**, 048002 (2022).
48. Norris, A. N., Shuvalov, A. L. & Kutsenko, A. A. Analytical formulation of three-dimensional dynamic homogenization for periodic elastic systems. *Proc. R. Soc. Lond. A* **468**, 1629–1651 (2012).
49. Nassar, H., He, Q.-C. & Auffray, N. A generalized theory of elastodynamic homogenization for periodic media. *Int. J. Solids Struct.* **84**, 139–146 (2016).
50. Meng, S. & Guzina, B. B. On the dynamic homogenization of periodic media: Willis' approach versus two-scale paradigm. *Proc. R. Soc. Lond. A* **474**, 20170638 (2018).
51. Willis, J. R. Exact effective relations for dynamics of a laminated body. *Mech. Mater.* **41**, 385–393 (2009).
52. Willis, J. R. Variational and related methods for the overall properties of composites. *Adv. Appl. Mech.* **21**, 1–78 (1981).
53. Willis, J. R. The construction of effective relations for waves in a composite. *C. R. Méc.* **340**, 181–192 (2012).
54. Milton, G. W., Briane, M. & Willis, J. R. On cloaking for elasticity and physical equations with a transformation invariant form. *New J. Phys.* **8**, 248 (2006).
55. Koo, S., Cho, C., Jeong, J.-h & Park, N. Acoustic omni meta-atom for decoupled access to all octants of a wave parameter space. *Nat. Commun.* **7**, 13012 (2016).
56. Sieck, C. F., Alù, A. & Haberman, M. R. Origins of Willis coupling and acoustic bianisotropy in acoustic metamaterials through source-driven homogenization. *Phys. Rev. B* **96**, 104303 (2017).

57. Fietz, C. & Shvets, G. Current-driven metamaterial homogenization. *Physica B* **405**, 2930–2934 (2010).
58. Kosmann-Schwarzbach, Y. & Schwarzbach, B. E. *The Noether Theorems: Invariance and Conservation Laws in the Twentieth Century* (Springer, 2011).
59. Bradley, C. & Cracknell, A. *The Mathematical Theory of Symmetry in Solids: Representation Theory for Point Groups and Space Groups* (Oxford Univ. Press, 2010).
60. Malgrange, C., Ricolleau, C. & Schlenker, M. *Symmetry and Physical Properties of Crystals* (Springer, 2014).
61. Dresselhaus, M. S., Dresselhaus, G. & Jorio, A. *Group Theory: Application to the Physics of Condensed Matter* (Springer, 2007).
62. Maugin, G. A. & Rousseau, M. *Wave Momentum and Quasi-Particles in Physical Acoustics* (World Scientific, 2015).
63. Maugin, G. A. *Material Inhomogeneities in Elasticity* (Springer, 1993).
64. Stone, M. *Phonons and Forces: Momentum Versus Pseudomomentum in Moving Fluids*, 335–363 (World Scientific, 2002).
65. Ziman, J. M. *Principles of the Theory of Solids* 2nd edn (Cambridge Univ. Press, 1979).
66. Brillouin, L. *Wave Propagation in Periodic Structures* (MGH, 1946).
67. Simon, S. *The Oxford Solid State Basics* (Oxford Univ. Press, 2013).
68. Laude, V., Achaoui, Y., Benchabane, S. & Khelif, A. Evanescent Bloch waves and the complex band structure of phononic crystals. *Phys. Rev. B* **80**, 092301 (2009).
69. Dwivedi, V. & Chua, V. Of bulk and boundaries: generalized transfer matrices for tight-binding models. *Phys. Rev. B* **93**, 134304 (2016).
70. Schomerus, H. *Random Matrix Approaches to Open Quantum Systems*, 409–473 (Oxford Univ. Press, 2017).
71. Markos, P. & Soukoulis, C. *Wave Propagation: From Electrons to Photonic Crystals and Left-Handed Materials* (Princeton Univ. Press, 2008).
72. Thomson, W. T. Transmission of elastic waves through a stratified solid medium. *J. Appl. Phys.* **21**, 89–93 (1950).
73. Banerjee, A., Das, R. & Calius, E. P. Waves in structured mediums or metamaterials: a review. *Arch. Comput. Methods Eng.* **26**, 1029–1058 (2018).
74. Novikov, S., Manakov, S. V., Pitaevskii, L. P. & Zakharov, V. E. *Theory of Solitons: The Inverse Scattering Method* (Springer, 1984).
75. Figotin, A. & Vitebskiy, I. Gigantic transmission band-edge resonance in periodic stacks of anisotropic layers. *Phys. Rev. E* **72**, 036619 (2005).
76. Saha, M., Agarwalla, B. K., Kulkarni, M. & Purkayastha, A. Universal subdiffusive behavior at band edges from transfer matrix exceptional points. *Phys. Rev. Lett.* **130**, 187101 (2023).
77. Saha, M., Agarwalla, B. K., Kulkarni, M. & Purkayastha, A. Effect of order of transfer matrix exceptional points on transport at band edges. *Phys. Rev. B* **111**, 125412 (2025).
78. Lustig, B., Elbaz, G., Muhafra, A. & Shmuel, G. Anomalous energy transport in laminates with exceptional points. *J. Mech. Phys. Solids* **133**, 103719 (2019).
79. Mokhtari, A. A., Lu, Y., Zhou, Q., Amirkhizi, A. V. & Srivastava, A. Scattering of in-plane elastic waves at metamaterial interfaces. *Int. J. Eng. Sci.* **150**, 103278 (2020).
80. Fishman, A., Elbaz, G., Varma, T. V. & Shmuel, G. Third-order exceptional points and frozen modes in planar elastic laminates. *J. Mech. Phys. Solids* **186**, 105590 (2024).
81. Shmuel, G. & Band, R. Universality of the frequency spectrum of laminates. *J. Mech. Phys. Solids* **92**, 127–136 (2016).
82. Lustig, B. & Shmuel, G. On the band gap universality of multiphase laminates and its applications. *J. Mech. Phys. Solids* **117**, 37–53 (2018).
83. Kaina, N., Lemoult, F., Fink, M. & Lerosey, G. Negative refractive index and acoustic superlens from multiple scattering in single negative metamaterials. *Nature* **525**, 77–81 (2015).
84. Lemoult, F., Kaina, N., Fink, M. & Lerosey, G. Soda cans metamaterial: a subwavelength-scaled phononic crystal. *Crystals* **6**, 82 (2016).
85. Yablonovitch, E. Photonic band-gap crystals. *J. Phys. Condens. Matter.* **5**, 2443–2460 (1993).
86. Watanabe, H. & Lu, L. Space group theory of photonic bands. *Phys. Rev. Lett.* **121**, 263903 (2018).
87. Maldovan, M. Sound and heat revolutions in phononics. *Nature* **503**, 209–217 (2013).
88. Khelif, A., Choujaa, A., Benchabane, S., Djafari-Rouhani, B. & Laude, V. Guiding and bending of acoustic waves in highly confined phononic crystal waveguides. *Appl. Phys. Lett.* **84**, 4400–4402 (2004).
89. Yang, S. et al. Focusing of sound in a 3D phononic crystal. *Phys. Rev. Lett.* **93**, 024301 (2004).
90. Ghaemsaidi, S. J., Fruchart, M. & Atis, S. Internal wave crystals. Preprint at https://arxiv.org/abs/2111.07984 (2021).
91. Ma, G. et al. Polarization bandgaps and fluid-like elasticity in fully solid elastic metamaterials. *Nat. Commun.* **7**, 13536 (2016).
92. Djafari-Rouhani, B., El-Jallal, S. & Pennec, Y. Phoxonic crystals and cavity optomechanics. *C. R. Phys.* **17**, 555–564 (2016).
93. Connes, A. *Noncommutative Geometry* (Academic, 1995).
94. Bellissard, J. in *From Number Theory to Physics* (eds Walldschmitdt, M., Moussa, P., Luck, J.-M. & Itzykson, C.) 538–630 (Springer, 1992).
95. Bellissard, J. *NCG Approach to Topological Invariants in Condensed Matter Physics: Lecture I* https://www.thp.uni-koeln.de/ESI-Web/slides/Bellissard-L1.pdf (2014).
96. Prodan, E. & Prodan, C. Topological phonon modes and their role in dynamic instability of microtubules. *Phys. Rev. Lett.* **103**, 248101 (2009).
97. Apigo, D. J., Cheng, W., Dobiszewski, K. F., Prodan, E. & Prodan, C. Observation of topological edge modes in a quasiperiodic acoustic waveguide. *Phys. Rev. Lett.* **122**, 095501 (2019).
98. Mitchell, N. P., Nash, L. M., Hexner, D., Turner, A. M. & Irvine, W. T. M. Amorphous topological insulators constructed from random point sets. *Nat. Phys.* **14**, 380–385 (2018).
99. Beli, D., Rosa, M. I. N., De Marqui Jr, C. & Ruzzene, M. Mechanics and dynamics of two-dimensional quasicrystalline composites. *Extreme Mech. Lett.* **44**, 101220 (2021).
100. Lai, Y., Zhang, X. & Zhang, Z.-Q. Large sonic band gaps in 12-fold quasicrystals. *J. Appl. Phys.* **91**, 6191–6193 (2002).
101. Martí-Sabaté, M. & Torrent, D. Edge modes for flexural waves in quasi-periodic linear arrays of scatterers. *APL Mater.* **9**, 081107 (2021).
102. Davies, B. & Craster, R. V. Symmetry-induced quasicrystalline waveguides. *Wave Motion* **115**, 103068 (2022).
103. Li, C. et al. Broadband asymmetric acoustic transmission by a plate with quasi-periodic surface ridges. *Appl. Phys. Lett.* **105**, 023511 (2014).
104. Ni, X. et al. Observation of Hofstadter butterfly and topological edge states in reconfigurable quasi-periodic acoustic crystals. *Commun. Phys.* **2**, 55 (2019).
105. Rosa, M. I., Guo, Y. & Ruzzene, M. Exploring topology of 1D quasiperiodic metastructures through modulated LEGO resonators. *Appl. Phys. Lett.* **118** (2021).
106. Davies, B., Chaplain, G. J., Starkey, T. A. & Craster, R. V. Graded quasiperiodic metamaterials perform fractal rainbow trapping. *Phys. Rev. Lett.* **131**, 177001 (2023).
107. Kaliteevski, M. et al. Tamm plasmon-polaritons: possible electromagnetic states at the interface of a metal and a dielectric Bragg mirror. *Phys. Rev. B* **76**, 165415 (2007).
108. Xiao, M., Zhang, Z. & Chan, C. T. Surface impedance and bulk band geometric phases in one-dimensional systems. *Phys. Rev. X* **4**, 021017 (2014).
109. Levy, E. & Akkermans, E. Topological boundary states in 1D: an effective Fabry–Perot model. *Eur. Phys. J. Spec. Top.* **226**, 1563–1582 (2017).
110. Hasan, M. Z. & Kane, C. L. Colloquium: topological insulators. *Rev. Mod. Phys.* **82**, 3045 (2010).
111. Yves, S., Ni, X. & Alù, A. Topological sound in two dimensions. *Ann. N.Y. Acad. Sci.* **1517**, 63–77 (2022).
112. Shankar, S., Souslov, A., Bowick, M. J., Marchetti, M. C. & Vitelli, V. Topological active matter. *Nat. Rev. Phys.* **4**, 380–398 (2022).
113. Ding, K., Fang, C. & Ma, G. Non-Hermitian topology and exceptional-point geometries. *Nat. Rev. Phys.* **4**, 745–760 (2022).
114. Zhu, W. et al. Topological phononic metamaterials. *Rep. Prog. Phys.* **86**, 106501 (2023).
115. Souslov, A., Dasbiswas, K., Fruchart, M., Vaikuntanathan, S. & Vitelli, V. Topological waves in fluids with odd viscosity. *Phys. Rev. Lett.* **122**, 128001 (2019).
116. Tauber, C., Delplace, P. & Venaille, A. A bulk-interface correspondence for equatorial waves. *J. Fluid Mech.* **868**, R2 (2019).
117. Tauber, C., Delplace, P. & Venaille, A. Anomalous bulk-edge correspondence in continuous media. *Phys. Rev. Res.* **2**, 013147 (2020).
118. Gangaraj, S. A. H. & Monticone, F. Physical violations of the bulk-edge correspondence in topological electromagnetics. *Phys. Rev. Lett.* **124**, 153901 (2020).
119. Zhong, J., Wang, H. & Fan, S. Pole and zero edge state invariant for one-dimensional non-Hermitian sublattice symmetry. *Phys. Rev. B* **110**, 214113 (2024).
120. Zhong, J., Wang, H., Poddubny, A. N. & Fan, S. Topological nature of edge states for one-dimensional systems without symmetry protection. *Phys. Rev. Lett.* **135**, 016601 (2025).
121. Pernas-Salomón, R., Haberman, M. R., Norris, A. N. & Shmuel, G. The electromomentum effect in piezoelectric Willis scatterers. *Wave Motion* **106**, 102797 (2021).
122. Liu, Y. et al. Willis metamaterial on a structured beam. *Phys. Rev. X* **9**, 011040 (2019).
123. Melnikov, A. et al. Acoustic meta-atom with experimentally verified maximum Willis coupling. *Nat. Commun.* **10**, 3148 (2019).
124. Quan, L., Ra'di, Y., Sounas, D. L. & Alù, A. Maximum Willis coupling in acoustic scatterers. *Phys. Rev. Lett.* **120**, 254301 (2018).
125. Merkel, A., Romero-García, V., Groby, J.-P., Li, J. & Christensen, J. Unidirectional zero sonic reflection in passive PT-symmetric Willis media. *Phys. Rev. B* **98**, 201102 (2018).
126. Peng, Y.-G., Mazor, Y. & Alù, A. Fundamentals of acoustic Willis media. *Wave Motion* **112**, 102930 (2022).
127. Esfahlani, H., Mazor, Y. & Alù, A. Homogenization and design of acoustic Willis metasurfaces. *Phys. Rev. B* **103**, 054306 (2021).
128. Lau, J., Tang, S. T., Yang, M. & Yang, Z. Coupled decorated membrane resonators with large Willis coupling. *Phys. Rev. Appl.* **12**, 014032 (2019).
129. Muhlestein, M. B., Sieck, C. F., Wilson, P. S. & Haberman, M. R. Experimental evidence of Willis coupling in a one-dimensional effective material element. *Nat. Commun.* **8**, 15625 (2017).
130. Sounas, D. L. & Alù, A. Extinction symmetry for reciprocal objects and its implications on cloaking and scattering manipulation. *Opt. Lett.* **39**, 4053–4056 (2014).
131. Lawrence, A. J., Goldsberry, B. M., Wallen, S. P. & Haberman, M. R. Numerical study of acoustic focusing using a bianisotropic acoustic lens. *J. Acoust. Soc. Am.* **148**, EL365–EL369 (2020).
132. Li, J. et al. Highly efficient generation of angular momentum with cylindrical bianisotropic metasurfaces. *Phys. Rev. Appl.* **11**, 024016 (2019).
133. Li, J., Shen, C., D'iaz-Rubio, A., Tretyakov, S. A. & Cummer, S. A. Systematic design and experimental demonstration of bianisotropic metasurfaces for scattering-free manipulation of acoustic wavefronts. *Nat. Commun.* **9**, 1342 (2018).
134. Hao, Y., Shen, Y., Groby, J.-P. & Li, J. Experimental demonstration of Willis coupling for elastic torsional waves. *Wave Motion* **112**, 102931 (2022).
135. Chen, Y. & Haberman, M. R. Controlling displacement fields in polar Willis solids via gauge transformations. *Phys. Rev. Lett.* **130**, 147201 (2023).
136. Sepehrirahnama, S., Oberst, S., Chiang, Y. K. & Powell, D. A. Willis coupling-induced acoustic radiation force and torque reversal. *Phys. Rev. Lett.* **129**, 174501 (2022).
137. Mason, W. P. *Piezoelectric Crystals and Their Application to Ultrasonics* (Van Nostrand, 1950).

138. Pernas-Salomón, R. & Shmuel, G. Symmetry breaking creates electro-momentum coupling in piezoelectric metamaterials. *J. Mech. Phys. Solids* **134**, 103770 (2020).
139. Muhafra, K., Haberman, M. R. & Shmuel, G. Discrete one-dimensional models for the electromomentum coupling. *Phys. Rev. Appl.* **20**, 014042 (2023).
140. Muhafra, A., Kosta, M., Torrent, D., Pernas-Salomón, R. & Shmuel, G. Homogenization of piezoelectric planar Willis materials undergoing antiplane shear. *Wave Motion* **108**, 102833 (2022).
141. Alù, A. Restoring the physical meaning of metamaterial constitutive parameters. *Phys. Rev. B* **83**, 081102 (2011).
142. Pernas-Salomón, R. & Shmuel, G. Fundamental principles for generalized Willis metamaterials. *Phys. Rev. Appl.* **14**, 064005 (2020).
143. Danawe, H. & Tol, S. Electro-momentum coupling tailored in piezoelectric metamaterials with resonant shunts. *APL Mater.* **11**, 091118 (2023).
144. Huynh, H. D. et al. Maximizing electro-momentum coupling in generalized 2D Willis metamaterials. *Extreme Mech. Lett.* **61**, 101981 (2023).
145. Lee, J.-H., Zhang, Z. & Gu, G. X. Maximum electro-momentum coupling in piezoelectric metamaterial scatterers. *J. Appl. Phys.* **132**, 125108 (2022).
146. Wallen, S. P., Casali, M. A., Goldsberry, B. M. & Haberman, M. R. Polarizability of electromomentum coupled scatterers. In *Proc. Meetings on Acoustics* https://doi.org/10.1121/2.0001597 (AIP, 2022).
147. Christensen, J. & de Abajo, F. J. G. Anisotropic metamaterials for full control of acoustic waves. *Phys. Rev. Lett.* **108**, 124301 (2012).
148. Oudich, M., Djafari-Rouhani, B., Pennec, Y., Assouar, M. B. & Bonello, B. Negative effective mass density of acoustic metamaterial plate decorated with low frequency resonant pillars. *J. Appl. Phys.* **116**, 184504 (2014).
149. Krishnamoorthy, H. N., Jacob, Z., Narimanov, E., Kretzschmar, I. & Menon, V. M. Topological transitions in metamaterials. *Science* **336**, 205–209 (2012).
150. Poddubny, A., Iorsh, I., Belov, P. & Kivshar, Y. Hyperbolic metamaterials. *Nat. Photon.* **7**, 948–957 (2013).
151. Gomez-Diaz, J. & Alù, A. Flatland optics with hyperbolic metasurfaces. *ACS Photon.* **3**, 2211–2224 (2016).
152. Huo, P., Zhang, S., Liang, Y., Lu, Y. & Xu, T. Hyperbolic metamaterials and metasurfaces: fundamentals and applications. *Adv. Opt. Mater.* **7**, 1801616 (2019).
153. Shen, C. et al. Broadband acoustic hyperbolic metamaterial. *Phys. Rev. Lett.* **115**, 254301 (2015).
154. Li, J., Fok, L., Yin, X., Bartal, G. & Zhang, X. Experimental demonstration of an acoustic magnifying hyperlens. *Nat. Mater.* **8**, 931–934 (2009).
155. Lu, D. & Liu, Z. Hyperlenses and metalenses for far-field super-resolution imaging. *Nat. Commun.* **3**, 1205 (2012).
156. Oh, J. H., Min Seung, H. & Young Kim, Y. A truly hyperbolic elastic metamaterial lens. *Appl. Phys. Lett.* **104**, 073503 (2014).
157. Zhu, R., Chen, Y., Wang, Y., Hu, G. & Huang, G. A single-phase elastic hyperbolic metamaterial with anisotropic mass density. *J. Acoust. Soc. Am.* **139**, 3303–3310 (2016).
158. Lee, H., Oh, J. H., Seung, H. M., Cho, S. H. & Kim, Y. Y. Extreme stiffness hyperbolic elastic metamaterial for total transmission subwavelength imaging. *Sci. Rep.* **6**, 24026 (2016).
159. Dong, H.-W., Zhao, S.-D., Wang, Y.-S. & Zhang, C. Broadband single-phase hyperbolic elastic metamaterials for super-resolution imaging. *Sci. Rep.* **8**, 2247 (2018).
160. Yves, S. et al. Moiré-driven topological transitions and extreme anisotropy in elastic metasurfaces. *Adv. Sci.* **9**, 2200181 (2022).
161. Quan, L. & Alù, A. Hyperbolic sound propagation over nonlocal acoustic metasurfaces. *Phys. Rev. Lett.* **123**, 244303 (2019).
162. Bliokh, K. Y. & Nori, F. Spin and orbital angular momenta of acoustic beams. *Phys. Rev. B* **99**, 174310 (2019).
163. Jones, W. L. Asymmetric wave-stress tensors and wave spin. *J. Fluid Mech.* **58**, 737–747 (1973).
164. Shi, C. et al. Observation of acoustic spin. *Natl Sci. Rev.* **6**, 707–712 (2019).
165. Burns, L., Bliokh, K. Y., Nori, F. & Dressel, J. Acoustic versus electromagnetic field theory: scalar, vector, spinor representations and the emergence of acoustic spin. *New J. Phys.* **22**, 053050 (2020).
166. Bliokh, K. Y. & Nori, F. Transverse spin and surface waves in acoustic metamaterials. *Phys. Rev. B* **99**, 020301 (2019).
167. Long, Y. et al. Symmetry selective directionality in near-field acoustics. *Natl Sci. Rev.* **7**, 1024–1035 (2020).
168. Long, Y., Yang, C., Chen, H. & Ren, J. Universal geometric relations of acoustic spin, energy flux, and reactive power. *Phys. Rev. Appl.* **19**, 064053 (2023).
169. Long, Y., Ren, J. & Chen, H. Intrinsic spin of elastic waves. *Proc. Natl Acad. Sci. USA* **115**, 9951–9955 (2018).
170. Bliokh, K. Y. Elastic spin and orbital angular momenta. *Phys. Rev. Lett.* **129**, 204303 (2022).
171. Chaplain, G., De Ponti, J. & Craster, R. Elastic orbital angular momentum. *Phys. Rev. Lett.* **128**, 064301 (2022).
172. Chaplain, G. J., De Ponti, J. M. & Starkey, T. A. Elastic orbital angular momentum transfer from an elastic pipe to a fluid. *Commun. Phys.* **5**, 279 (2022).
173. Wang, S., Ma, G. & Chan, C. T. Topological transport of sound mediated by spin-redirection geometric phase. *Sci. Adv.* **4**, eaaq1475 (2018).
174. Jiang, X., Li, Y., Liang, B., Cheng, J.-c & Zhang, L. Convert acoustic resonances to orbital angular momentum. *Phys. Rev. Lett.* **117**, 034301 (2016).
175. Fu, Y. et al. Sound vortex diffraction via topological charge in phase gradient metagratings. *Sci. Adv.* **6**, eaba9876 (2020).
176. Gao, S., Li, Y., Ma, C., Cheng, Y. & Liu, X. Emitting long-distance spiral airborne sound using low-profile planar acoustic antenna. *Nat. Commun.* **12**, 2006 (2021).
177. Fan, X.-D. & Zhang, L. Acoustic orbital angular momentum Hall effect and realization using a metasurface. *Phys. Rev. Res.* **3**, 013251 (2021).
178. Jiang, X., Ta, D. & Wang, W. Modulation of orbital-angular-momentum symmetry of nondiffractive acoustic vortex beams and realization using a metasurface. *Phys. Rev. Appl.* **14**, 034014 (2020).
179. Zhang, H. et al. Topologically crafted spatiotemporal vortices in acoustics. *Nat. Commun.* **14**, 6238 (2023).
180. Wang, Q. et al. Vortex states in an acoustic Weyl crystal with a topological lattice defect. *Nat. Commun.* **12**, 3654 (2021).
181. Lu, J., Qiu, C., Ke, M. & Liu, Z. Valley vortex states in sonic crystals. *Phys. Rev. Lett.* **116**, 093901 (2016).
182. Long, Y. et al. Realization of acoustic spin transport in metasurface waveguides. *Nat. Commun.* **11**, 4716 (2020).
183. Frenzel, T., Kadic, M. & Wegener, M. Three-dimensional mechanical metamaterials with a twist. *Science* **358**, 1072–1074 (2017).
184. Frenzel, T., Köpfler, J., Jung, E., Kadic, M. & Wegener, M. Ultrasound experiments on acoustical activity in chiral mechanical metamaterials. *Nat. Commun.* **10**, 3384 (2019).
185. Chen, Y., Kadic, M., Guenneau, S. & Wegener, M. Isotropic chiral acoustic phonons in 3D quasicrystalline metamaterials. *Phys. Rev. Lett.* **124**, 235502 (2020).
186. Wang, S. et al. Spin-orbit interactions of transverse sound. *Nat. Commun.* **12**, 6125 (2021).
187. Noetinger, G. et al. Superresolved imaging based on spatiotemporal wave-front shaping. *Phys. Rev. Appl.* **19**, 024032 (2023).
188. Shi, C., Dubois, M., Wang, Y. & Zhang, X. High-speed acoustic communication by multiplexing orbital angular momentum. *Proc. Natl Acad. Sci. USA* **114**, 7250–7253 (2017).
189. Baresch, D., Thomas, J.-L. & Marchiano, R. Observation of a single-beam gradient force acoustical trap for elastic particles: acoustical tweezers. *Phys. Rev. Lett.* **116**, 024301 (2016).
190. Melde, K., Mark, A. G., Qiu, T. & Fischer, P. Holograms for acoustics. *Nature* **537**, 518–522 (2016).
191. Cox, L., Melde, K., Croxford, A., Fischer, P. & Drinkwater, B. W. Acoustic hologram enhanced phased arrays for ultrasonic particle manipulation. *Phys. Rev. Appl.* **12**, 064055 (2019).
192. Melde, K. et al. Compact holographic sound fields enable rapid one-step assembly of matter in 3D. *Sci. Adv.* **9**, eadf6182 (2023).
193. Maznev, A., Every, A. & Wright, O. Reciprocity in reflection and transmission: what is a 'phonon diode'? *Wave Motion* **50**, 776–784 (2013).
194. Buddhiraju, S., Song, A., Papadakis, G. T. & Fan, S. Nonreciprocal metamaterial obeying time-reversal symmetry. *Phys. Rev. Lett.* **124**, 257403 (2020).
195. Guo, C., Zhao, Z. & Fan, S. Internal transformations and internal symmetries in linear photonic systems. *Phys. Rev. A* **105**, 023509 (2022).
196. Zangeneh-Nejad, F. & Fleury, R. Active times for acoustic metamaterials. *Rev. Phys.* **4**, 100031 (2019).
197. Caloz, C. et al. Electromagnetic nonreciprocity. *Phys. Rev. Appl.* **10**, 047001 (2018).
198. Asadchy, V. S., Mirmoosa, M. S., Díaz-Rubio, A., Fan, S. & Tretyakov, S. A. Tutorial on electromagnetic nonreciprocity and its origins. *Proc. IEEE* **108**, 1684–1727 (2020).
199. Cummer, S. A. Selecting the direction of sound transmission. *Science* **343**, 495–496 (2014).
200. Lüthi, B. *Physical Acoustics in the Solid State* 1st edn (Springer, 2005).
201. Kittel, C. Interaction of spin waves and ultrasonic waves in ferromagnetic crystals. *Phys. Rev.* **110**, 836 (1958).
202. Lewis, M. F. & Patterson, E. Acoustic-surface-wave isolator. *Appl. Phys. Lett.* **20**, 276–278 (1972).
203. Heil, J., Lüthi, B. & Thalmeier, P. Nonreciprocal surface-acoustic-wave propagation in aluminum. *Phys. Rev. B* **25**, 6515–6517 (1982).
204. Verba, R., Lisenkov, I., Krivorotov, I., Tiberkevich, V. & Slavin, A. Nonreciprocal surface acoustic waves in multilayers with magnetoelastic and interfacial Dzyaloshinskii-Moriya interactions. *Phys. Rev. Appl.* **9**, 064014 (2018).
205. Verba, R., Tiberkevich, V. & Slavin, A. Wide-band nonreciprocity of surface acoustic waves induced by magnetoelastic coupling with a synthetic antiferromagnet. *Phys. Rev. Appl.* **12**, 054061 (2019).
206. Shah, P. J. et al. Giant nonreciprocity of surface acoustic waves enabled by the magnetoelastic interaction. *Sci. Adv.* https://doi.org/10.1126/sciadv.abc5648 (2020).
207. Godin, O. A. Reciprocity and energy theorems for waves in a compressible inhomogeneous moving fluid. *Wave Motion* **25**, 143–167 (1997).
208. Brekhovskikh, L. M. & Godin, O. A. *Acoustics of Layered Media II: Point Sources and Bounded Beams* 2nd edn (Springer, 1999).
209. Morse, P. M. & Ingard, K. U. *Theoretical Acoustics* (McGraw-Hill, 1968).
210. Silbiger, O. & Hadad, Y. One-way acoustic guiding under transverse fluid flow. *Phys. Rev. Appl.* **17**, 064058 (2022).
211. Roux, P., de Rosny, J., Tanter, M. & Fink, M. The Aharonov–Bohm effect revisited by an acoustic time-reversal mirror. *Phys. Rev. Lett.* **79**, 3170 (1997).
212. Fleury, R., Sounas, D. L., Sieck, C. F., Haberman, M. R. & Alù, A. Sound isolation and giant linear nonreciprocity in a compact acoustic circulator. *Science* **343**, 516–519 (2014).
213. Fleury, R. *Breaking Temporal Symmetries in Metamaterials and Metasurfaces*. PhD thesis, Univ. Texas Austin (2015).
214. Khanikaev, A. B., Fleury, R., Mousavi, S. H. & Alù, A. Topologically robust sound propagation in an angular-momentum-biased graphene-like resonator lattice. *Nat. Commun.* **6**, 8260 (2015).
215. Ding, Y. et al. Experimental demonstration of acoustic Chern insulators. *Phys. Rev. Lett.* **122**, 014302 (2019).
216. Zhang, Z., Delplace, P. & Fleury, R. Superior robustness of anomalous non-reciprocal topological edge states. *Nature* **598**, 293–297 (2021).

217. Zhu, Y. et al. Janus acoustic metascreen with nonreciprocal and reconfigurable phase modulations. *Nat. Commun.* **12**, 7089 (2021).
218. Goldsberry, B. M., Wallen, S. P. & Haberman, M. R. Nonreciprocity and mode conversion in a spatiotemporally modulated elastic wave circulator. *Phys. Rev. Appl.* **17**, 034050 (2022).
219. Jorge, C., Chardac, A., Poncet, A. & Bartolo, D. Active hydraulics laws from frustration principles. *Nat. Phys.* **20**, 303–309 (2024).
220. Yang, X., Ren, C., Cheng, K. & Zhang, H. P. Robust boundary flow in chiral active fluid. *Phys. Rev. E* **101**, 022603 (2020).
221. Souslov, A., van Zuiden, B. C., Bartolo, D. & Vitelli, V. Topological sound in active-liquid metamaterials. *Nat. Phys.* **13**, 1091–1094 (2017).
222. Quan, L., Yves, S., Peng, Y., Esfahlani, H. & Alù, A. Odd Willis coupling induced by broken time-reversal symmetry. *Nat. Commun.* **12**, 2615 (2021).
223. Liang, B., Guo, X., Tu, J., Zhang, D. & Cheng, J. An acoustic rectifier. *Nat. Mater.* **9**, 989–992 (2010).
224. Blanchard, A., Sapsis, T. P. & Vakakis, A. F. Non-reciprocity in nonlinear elastodynamics. *J. Sound Vib.* **412**, 326–335 (2018).
225. Sounas, D. L. & Alù, A. Time-reversal symmetry bounds on the electromagnetic response of asymmetric structures. *Phys. Rev. Lett.* **118**, 154302 (2017).
226. Darabi, A. et al. Broadband passive nonlinear acoustic diode. *Phys. Rev. B* **99**, 214305 (2019).
227. Devaux, T., Cebrecos, A., Richoux, O., Pagneux, V. & Tournat, V. Acoustic radiation pressure for nonreciprocal transmission and switch effects. *Nat. Commun.* **10**, 3292 (2019).
228. Liang, B., Yuan, B. & Cheng, J.-c Acoustic diode: rectification of acoustic energy flux in one-dimensional systems. *Phys. Rev. Lett.* **103**, 104301 (2009).
229. Liu, C., Du, Z., Sun, Z., Gao, H. & Guo, X. Frequency-preserved acoustic diode model with high forward-power-transmission rate. *Phys. Rev. Appl.* **3**, 064014 (2015).
230. Cui, J.-G., Yang, T. & Chen, L.-Q. Frequency-preserved non-reciprocal acoustic propagation in a granular chain. *Appl. Phys. Lett.* **112**, 181904 (2018).
231. Boechler, N., Theocharis, G. & Daraio, C. Bifurcation-based acoustic switching and rectification. *Nat. Mater.* **10**, 665–668 (2011).
232. Meng, X. & Liu, S. Roton-enabled mechanical diode at extremely low frequency. *J. Appl. Mech.* **91**, 011010–1 (2024).
233. Guo, X., Lissek, H. & Fleury, R. Observation of non-reciprocal harmonic conversion in real sounds. *Commun. Phys.* **6**, 93 (2023).
234. Devaux, T., Tournat, V., Richoux, O. & Pagneux, V. Asymmetric acoustic propagation of wave packets via the self-demodulation effect. *Phys. Rev. Lett.* **115**, 234301 (2015).
235. Fang, L., Mojahed, A., Darabi, A., Vakakis, A. F. & Leamy, M. J. Passive nonreciprocity in a system of asymmetrical rotational oscillators. *Phys. Rev. Appl.* **15**, 034005 (2021).
236. Librandi, G., Tubaldi, E. & Bertoldi, K. Programming nonreciprocity and reversibility in multistable mechanical metamaterials. *Nat. Commun.* **12**, 3454 (2021).
237. Muhlestein, M. B., Sieck, C. F., Alù, A. & Haberman, M. R. Reciprocity, passivity and causality in Willis materials. *Proc. R. Soc. Lond. A* http://rspa.royalsocietypublishing.org/content/472/2194/20160604 (2016).
238. Christensen, J., Haberman, M. R., Srivastava, A., Huang, G. & Shmuel, G. Perspective on non-Hermitian elastodynamics. *Appl. Phys. Lett.* **125**, 230501 (2024).
239. Wu, Q. et al. Active metamaterials for realizing odd mass density. *Proc. Natl Acad. Sci. USA* **120**, e2209829120 (2023).
240. Quan, L., Sounas, D. L. & Alù, A. Nonreciprocal Willis coupling in zero-index moving media. *Phys. Rev. Lett.* **123**, 064301 (2019).
241. Beatus, T., Tlusty, T. & Bar-Ziv, R. Phonons in a one-dimensional microfluidic crystal. *Nat. Phys.* **2**, 743–748 (2006).
242. Beatus, T., Bar-Ziv, R. H. & Tlusty, T. The physics of 2D microfluidic droplet ensembles. *Phys. Rep.* **516**, 103–145 (2012).
243. Cho, C., Wen, X., Park, N. & Li, J. Acoustic Willis meta-atom beyond the bounds of passivity and reciprocity. *Commun. Phys.* **4**, 82 (2021).
244. Wen, X., Yip, H. K., Cho, C., Li, J. & Park, N. Acoustic amplifying diode using nonreciprocal Willis coupling. *Phys. Rev. Lett.* **130**, 176101 (2023).
245. Zhai, Y., Kwon, H.-S. & Popa, B.-I. Active willis metamaterials for ultracompact nonreciprocal linear acoustic devices. *Phys. Rev. B* **99**, 220301 (2019).
246. Chen, Y., Li, X., Hu, G., Haberman, M. R. & Huang, G. An active mechanical Willis meta-layer with asymmetric polarizabilities. *Nat. Commun.* **11**, 3681 (2020).
247. Nassar, H., Xu, X., Norris, A. & Huang, G. Modulated phononic crystals: non-reciprocal wave propagation and Willis materials. *J. Mech. Phys. Solids* **101**, 10–29 (2017).
248. Olivier, C. et al. Nonreciprocal and even Willis couplings in periodic thermoacoustic amplifiers. *Phys. Rev. B* **104**, 184109 (2021).
249. Avron, J. Odd viscosity. *J. Stat. Phys.* **92**, 543–557 (1998).
250. Fruchart, M., Scheibner, C. & Vitelli, V. Odd viscosity and odd elasticity. *Annu. Rev. Condens. Matter Phys.* **14**, 471–510 (2023).
251. Heidari, S., Cortijo, A. & Asgari, R. Hall viscosity for optical phonons. *Phys. Rev. B* **100**, 165427 (2019).
252. Barkeshli, M., Chung, S. B. & Qi, X.-L. Dissipationless phonon Hall viscosity. *Phys. Rev. B* **85**, 245107 (2012).
253. Flebus, B. & MacDonald, A. Phonon Hall viscosity of ionic crystals. *Phys. Rev. Lett.* **131**, 236301 (2023).
254. Han, M. et al. Fluctuating hydrodynamics of chiral active fluids. *Nat. Phys.* **17**, 1260–1269 (2021).
255. Soni, V. et al. The odd free surface flows of a colloidal chiral fluid. *Nat. Phys.* **15**, 1188–1194 (2019).
256. Sone, K. & Ashida, Y. Anomalous topological active matter. *Phys. Rev. Lett.* **123**, 205502 (2019).
257. Khain, T., Scheibner, C., Fruchart, M. & Vitelli, V. Stokes flows in three-dimensional fluids with odd and parity-violating viscosities. *J. Fluid Mech.* https://doi.org/10.1017/jfm.2021.1079 (2022).
258. Markovich, T. & Lubensky, T. C. Nonreciprocity and odd viscosity in chiral active fluids. *Proc. Natl Acad. Sci. USA* **121**, e2219385121 (2024).
259. Hosaka, Y., Komura, S. & Andelman, D. Nonreciprocal response of a two-dimensional fluid with odd viscosity. *Phys. Rev. E* **103**, 042610 (2021).
260. Hosaka, Y., Golestanian, R. & Vilfan, A. Lorentz reciprocal theorem in fluids with odd viscosity. *Phys. Rev. Lett.* **131**, 178303 (2023).
261. de Wit, X. M., Fruchart, M., Khain, T., Toschi, F. & Vitelli, V. Pattern formation by turbulent cascades. *Nature* **627**, 515–521 (2024).
262. Chen, S. et al. Chirality across scales in tissue dynamics. Preprint at https://arxiv.org/abs/2506.12276 (2025).
263. Floquet, G. Sur les équations différentielles linéaires à coefficients périodiques. *Ann. Sci. Éc. Norm. Supér.* **12**, 47–88 (1883).
264. Rahav, S., Gilary, I. & Fishman, S. Effective Hamiltonians for periodically driven systems. *Phys. Rev. A* **68**, 013820 (2003).
265. Goldman, N. & Dalibard, J. Periodically driven quantum systems: effective Hamiltonians and engineered gauge fields. *Phys. Rev. X* **4**, 031027 (2014).
266. Rudner, M. S. & Lindner, N. H. The Floquet engineer's handbook. Preprint at https://doi.org/10.48550/arXiv.2003.08252 (2020).
267. Khemani, V., Moessner, R. & Sondhi, S. L. A brief history of time crystals. Preprint at https://arxiv.org/abs/1910.10745 (2019).
268. Zaletel, M. P. et al. Colloquium: Quantum and classical discrete time crystals. *Rev. Mod. Phys.* **95**, 031001 (2023).
269. Yao, N. Y., Nayak, C., Balents, L. & Zaletel, M. P. Classical discrete time crystals. *Nat. Phys.* **16**, 438–447 (2020).
270. Avni, Y., Fruchart, M., Martin, D., Seara, D. & Vitelli, V. Nonreciprocal Ising model. *Phys. Rev. Lett.* **134**, 117103 (2025).
271. Izhikevich, E. *Dynamical Systems in Neuroscience* (MIT Press, 2007).
272. Winfree, A. T. *The Geometry of Biological Time* (Springer, 2001).
273. Sambe, H. Steady states and quasienergies of a quantum-mechanical system in an oscillating field. *Phys. Rev. A* **7**, 2203 (1973).
274. Fleury, R., Khanikaev, A. B. & Alù, A. Floquet topological insulators for sound. *Nat. Commun.* **7**, 11744 (2016).
275. Trainiti, G. et al. Time-periodic stiffness modulation in elastic metamaterials for selective wave filtering: theory and experiment. *Phys. Rev. Lett.* **122**, 124301 (2019).
276. Disa, A. S., Nova, T. F. & Cavalleri, A. Engineering crystal structures with light. *Nat. Phys.* **17**, 1087–1092 (2021).
277. Juraschek, D. M., Neuman, T. & Narang, P. Giant effective magnetic fields from optically driven chiral phonons in *4f* paramagnets. *Phys. Rev. Res.* **4**, 013129 (2022).
278. Shin, D. et al. Phonon-driven spin-Floquet magneto-valleytronics in MoS_2. *Nat. Commun.* **9**, 638 (2018).
279. Radaelli, P. G. Breaking symmetry with light: ultrafast ferroelectricity and magnetism from three-phonon coupling. *Phys. Rev. B* **97**, 085145 (2018).
280. Fleury, R., Sounas, D. L. & Alù, A. Subwavelength ultrasonic circulator based on spatiotemporal modulation. *Phys. Rev. B* **91**, 174306 (2015).
281. Shen, C., Zhu, X., Li, J. & Cummer, S. A. Nonreciprocal acoustic transmission in space-time modulated coupled resonators. *Phys. Rev. B* **100**, 054302 (2019).
282. Chen, Y. et al. Nonreciprocal wave propagation in a continuum-based metamaterial with space-time modulated resonators. *Phys. Rev. Appl.* **11**, 064052 (2019).
283. Wang, Y. et al. Observation of nonreciprocal wave propagation in a dynamic phononic lattice. *Phys. Rev. Lett.* **121**, 194301 (2018).
284. Marconi, J. et al. Experimental observation of nonreciprocal band gaps in a space-time-modulated beam using a shunted piezoelectric array. *Phys. Rev. Appl.* **13**, 031001 (2020).
285. Chen, Z. et al. Efficient nonreciprocal mode transitions in spatiotemporally modulated acoustic metamaterials. *Sci. Adv.* **7**, eabj1198 (2021).
286. Shao, L. et al. Electrical control of surface acoustic waves. *Nat. Electron.* **5**, 348–355 (2022).
287. Wen, X. et al. Unidirectional amplification with acoustic non-Hermitian space-time varying metamaterial. *Commun. Phys.* **5**, 18 (2022).
288. Darabi, A., Ni, X., Leamy, M. & Alù, A. Reconfigurable Floquet elastodynamic topological insulator based on synthetic angular momentum bias. *Sci. Adv.* **6**, eaba8656 (2020).
289. Chen, Z.-x et al. Observation of acoustic Floquet π modes in a time-varying lattice. *Phys. Rev. B* **109**, L020302 (2024).
290. Peng, Y.-G. et al. Chirality-assisted three-dimensional acoustic Floquet lattices. *Phys. Rev. Res.* **1**, 033149 (2019).
291. Zhu, W., Xue, H., Gong, J., Chong, Y. & Zhang, B. Time-periodic corner states from Floquet higher-order topology. *Nat. Commun.* **13**, 11 (2022).
292. Cheng, Z. et al. Observation of π/2 modes in an acoustic Floquet system. *Phys. Rev. Lett.* **129**, 254301 (2022).
293. Caloz, C. & Deck-Leger, Z.-L. Spacetime metamaterials, Part II: theory and applications. *IEEE Trans. Antennas Propag.* **68**, 1583–1598 (2019).
294. Liberal, I., Ganfornina-Andrades, A. & Vázquez-Lozano, J. E. Spatiotemporal symmetries and energy-momentum conservation in uniform spacetime metamaterials. *ACS Photon.* **11**, 5273–5280 (2024).
295. Bacot, V., Labousse, M., Eddi, A., Fink, M. & Fort, E. Time reversal and holography with spacetime transformations. *Nat. Phys.* **12**, 972–977 (2016).

296. Bacot, V., Durey, G., Eddi, A., Fink, M. & Fort, E. Phase-conjugate mirror for water waves driven by the Faraday instability. *Proc. Natl Acad. Sci. USA* **116**, 8809–8814 (2019).
297. Mouet, V., Apffel, B. & Fort, E. Comprehensive refractive manipulation of water waves using electrostriction. *Proc. Natl Acad. Sci. USA* **120**, e2216828120 (2023).
298. Apffel, B., Wildeman, S., Eddi, A. & Fort, E. Experimental implementation of wave propagation in disordered time-varying media. *Phys. Rev. Lett.* **128**, 094503 (2022).
299. Fink, M. et al. Time-reversed acoustics. *Rep. Prog. Phys.* **63**, 1933–1995 (2000).
300. Lanoy, M., Lemoult, F., Eddi, A. & Prada, C. Dirac cones and chiral selection of elastic waves in a soft strip. *Proc. Natl Acad. Sci. USA* **117**, 30186–30190 (2020).
301. Delory, A., Lemoult, F., Lanoy, M., Eddi, A. & Prada, C. Soft elastomers: a playground for guided waves. *J. Acoust. Soc. Am.* **151**, 3343–3358 (2022).
302. Delory, A., Lemoult, F., Eddi, A. & Prada, C. Guided elastic waves in a highly-stretched soft plate. *Extreme Mech. Lett.* **61**, 102018 (2023).
303. Delory, A. et al. Elastic wave packets crossing a space-time interface. *Phys. Rev. Lett.* **133**, 267201 (2024).
304. Ashida, Y., Gong, Z. & Ueda, M. Non-Hermitian physics. *Adv. Phys.* **69**, 249–435 (2020).
305. Bender, C. M. & Boettcher, S. Real spectra in non-Hermitian Hamiltonians having *PT* symmetry. *Phys. Rev. Lett.* **80**, 5243 (1998).
306. Bender, C. M., Berry, M. V. & Mandilara, A. Generalized PT symmetry and real spectra. *J. Phys. A* **35**, L467–L471 (2002).
307. Mostafazadeh, A. in *Geometric Methods in Physics* (eds Kielanowski, P., Bieliavsky, P., Odzijewicz, A., Schlichenmaier, M. & Voronov, T.) 145–165 (Springer, 2015).
308. Li, Y. et al. Anti–parity-time symmetry in diffusive systems. *Science* **364**, 170–173 (2019).
309. Peng, P. et al. Anti-parity–time symmetry with flying atoms. *Nat. Phys.* **12**, 1139–1145 (2016).
310. Zhu, X., Ramezani, H., Shi, C., Zhu, J. & Zhang, X. *PT*-symmetric acoustics. *Phys. Rev. X* **4**, 031042 (2014).
311. Christensen, J., Willatzen, M., Velasco, V. & Lu, M.-H. Parity-time synthetic phononic media. *Phys. Rev. Lett.* **116**, 207601 (2016).
312. Fleury, R., Sounas, D. L. & Alù, A. Parity-time symmetry in acoustics: theory, devices, and potential applications. *IEEE J. Sel. Top. Quantum Electron.* **22**, 121–129 (2016).
313. Shi, C. et al. Accessing the exceptional points of parity-time symmetric acoustics. *Nat. Commun.* **7**, 11110 (2016).
314. Ding, K., Ma, G., Xiao, M., Zhang, Z. & Chan, C. T. Emergence, coalescence, and topological properties of multiple exceptional points and their experimental realization. *Phys. Rev. X* **6**, 021007 (2016).
315. Ding, K., Ma, G., Zhang, Z. & Chan, C. T. Experimental demonstration of an anisotropic exceptional point. *Phys. Rev. Lett.* **121**, 085702 (2018).
316. Tang, W. et al. Exceptional nexus with a hybrid topological invariant. *Science* **370**, 1077–1080 (2020).
317. Tang, W., Ding, K. & Ma, G. Direct measurement of topological properties of an exceptional parabola. *Phys. Rev. Lett.* **127**, 034301 (2021).
318. Tang, W., Ding, K. & Ma, G. Realization and topological properties of third-order exceptional lines embedded in exceptional surfaces. *Nat. Commun.* **14**, 6660 (2023).
319. Elbaz, G., Pick, A., Moiseyev, N. & Shmuel, G. Encircling exceptional points of bloch waves: mode conversion and anomalous scattering. *J. Phys. D* http://iopscience.iop.org/article/10.1088/1361-6463/ac5859 (2022).
320. Achilleos, V., Theocharis, G., Richoux, O. & Pagneux, V. Non-Hermitian acoustic metamaterials: role of exceptional points in sound absorption. *Phys. Rev. B* **95**, 144303 (2017).
321. Shmuel, G. & Moiseyev, N. Linking scalar elastodynamics and non-Hermitian quantum mechanics. *Phys. Rev. Appl.* **13**, 024074 (2020).
322. Wiersig, J. Review of exceptional point-based sensors. *Photonics Res.* **8**, 1457 (2020).
323. Ge, L., Chong, Y. & Stone, A. D. Conservation relations and anisotropic transmission resonances in one-dimensional *PT*-symmetric photonic heterostructures. *Phys. Rev. A* **85**, 023802 (2012).
324. Fleury, R., Sounas, D. & Alù, A. An invisible acoustic sensor based on parity-time symmetry. *Nat. Commun.* **6**, 5905 (2015).
325. Rivet, E. et al. Constant-pressure sound waves in non-Hermitian disordered media. *Nat. Phys.* **14**, 942–947 (2018).
326. Li, H.-x. et al. Ultrathin acoustic parity-time symmetric metasurface cloak. *Research* https://doi.org/10.34133/2019/8345683 (2019).
327. Magariyachi, T., Arias Casals, H., Herrero, R., Botey, M. & Staliunas, K. PT-symmetric Helmholtz resonator dipoles for sound directivity. *Phys. Rev. B* **103**, 094201 (2021).
328. Krasnok, A. et al. Anomalies in light scattering. *Adv. Opt. Photon.* **11**, 892–951 (2019).
329. Kim, S., Krasnok, A. & Alù, A. Complex-frequency excitations in photonics and wave physics. *Science* **387**, eado4128 (2025).
330. Baranov, D. G., Krasnok, A. & Alù, A. Coherent virtual absorption based on complex zero excitation for ideal light capturing. *Optica* **4**, 1457–1461 (2017).
331. Kim, S., Lepeshov, S., Krasnok, A. & Alù, A. Beyond bounds on light scattering with complex frequency excitations. *Phys. Rev. Lett.* **129**, 203601 (2022).
332. Ra'di, Y., Krasnok, A. & Alú, A. Virtual critical coupling. *ACS Photon.* **7**, 1468–1475 (2020).
333. Trainiti, G., Ra'di, Y., Ruzzene, M. & Alù, A. Coherent virtual absorption of elastodynamic waves. *Sci. Adv.* **5**, eaaw3255 (2019).
334. Rasmussen, C., Rosa, M. I., Lewton, J. & Ruzzene, M. A lossless sink based on complex frequency excitations. *Adv. Sci.* **10**, 2301811 (2023).
335. Gu, Z. et al. Transient non-Hermitian skin effect. *Nat. Commun.* **13**, 7668 (2022).
336. Kim, S., Peng, Y.-G., Yves, S. & Alù, A. Loss compensation and superresolution in metamaterials with excitations at complex frequencies. *Phys. Rev. X* **13**, 041024 (2023).
337. Vahala, K. et al. A phonon laser. *Nat. Phys.* **5**, 682–686 (2009).
338. Grudinin, I. S., Lee, H., Painter, O. & Vahala, K. J. Phonon laser action in a tunable two-level system. *Phys. Rev. Lett.* **104**, 083901 (2010).
339. Jing, H. et al. PT-symmetric phonon laser. *Phys. Rev. Lett.* **113**, 053604 (2014).
340. Jiang, Y., Maayani, S., Carmon, T., Nori, F. & Jing, H. Nonreciprocal phonon laser. *Phys. Rev. Appl.* **10**, 064037 (2018).
341. Zhang, J. et al. A phonon laser operating at an exceptional point. *Nat. Photon.* **12**, 479–484 (2018).
342. Behrle, T. et al. Phonon laser in the quantum regime. *Phys. Rev. Lett.* **131**, 043605 (2023).
343. Pedergnana, T., Faure-Beaulieu, A., Fleury, R. & Noiray, N. Loss-compensated non-reciprocal scattering based on synchronization. *Nat. Commun.* **15**, 7436 (2024).
344. Pedergnana, T. & Noiray, N. Superradiant scattering by a limit cycle. *Phys. Rev. Appl.* **20**, 034068 (2023).
345. Patil, G. U. & Matlack, K. H. Review of exploiting nonlinearity in phononic materials to enable nonlinear wave responses. *Acta Mech.* **233**, 1–46 (2021).
346. Manktelow, K. L., Ruzzene, M. & Leamy, M. J. in *Dynamics of Lattice Materials* (eds Phani, A. S. & Hussein, M. I.) 107–137 (Wiley, 2017).
347. Hatano, N. & Nelson, D. R. Localization transitions in non-Hermitian quantum mechanics. *Phys. Rev. Lett.* **77**, 570 (1996).
348. Kawabata, K., Shiozaki, K., Ueda, M. & Sato, M. Symmetry and topology in non-Hermitian physics. *Phys. Rev. X* **9**, 041015 (2019).
349. Hu, Y.-M., Huang, Y.-Q., Xue, W.-T. & Wang, Z. Non-Bloch band theory for non-Hermitian continuum systems. *Phys. Rev. B* **110**, 205429 (2024).
350. Ghatak, A., Brandenbourger, M., Van Wezel, J. & Coulais, C. Observation of non-Hermitian topology and its bulk–edge correspondence in an active mechanical metamaterial. *Proc. Natl Acad. Sci. USA* **117**, 29561–29568 (2020).
351. Gao, P., Willatzen, M. & Christensen, J. Anomalous topological edge states in non-Hermitian piezophononic media. *Phys. Rev. Lett.* **125**, 206402 (2020).
352. Zhang, L. et al. Acoustic non-Hermitian skin effect from twisted winding topology. *Nat. Commun.* **12**, 6297 (2021).
353. Zhang, X., Tian, Y., Jiang, J.-H., Lu, M.-H. & Chen, Y.-F. Observation of higher-order non-Hermitian skin effect. *Nat. Commun.* **12**, 5377 (2021).
354. Wang, W., Wang, X. & Ma, G. Non-Hermitian morphing of topological modes. *Nature* **608**, 50–55 (2022).
355. Wang, W., Hu, M., Wang, X., Ma, G. & Ding, K. Experimental realization of geometry-dependent skin effect in a reciprocal two-dimensional lattice. *Phys. Rev. Lett.* **131**, 207201 (2023).
356. Scheibner, C., Irvine, W. T. & Vitelli, V. Non-Hermitian band topology and skin modes in active elastic media. *Phys. Rev. Lett.* **125**, 118001 (2020).
357. Wang, Y., Wu, Q., Tian, Y. & Huang, G. Non-Hermitian wave dynamics of odd plates: microstructure design and theoretical modelling. *J. Mech. Phys. Solids* **182**, 105462 (2024).
358. Franca, S., Könye, V., Hassler, F., van den Brink, J. & Fulga, C. Non-Hermitian physics without gain or loss: the skin effect of reflected waves. *Phys. Rev. Lett.* **129**, 086601 (2022).
359. Chen, Y., Li, X., Scheibner, C., Vitelli, V. & Huang, G. Realization of active metamaterials with odd micropolar elasticity. *Nat. Commun.* **12**, 5935 (2021).
360. Veenstra, J. et al. Adaptive locomotion of active solids. *Nature* **639**, 935–941 (2025).
361. Fossati, M., Scheibner, C., Fruchart, M. & Vitelli, V. Odd elasticity and topological waves in active surfaces. *Phys. Rev. E* **109**, 024608 (2024).
362. Bradlyn, B. et al. Topological quantum chemistry. *Nature* **547**, 298–305 (2017).
363. Cano, J. & Bradlyn, B. Band representations and topological quantum chemistry. *Annu. Rev. Condens. Matter Phys.* **12**, 225–246 (2021).
364. Xu, Y. et al. Catalog of topological phonon materials. *Science* **384**, eadf8458 (2024).
365. Lu, J. et al. Observation of topological valley transport of sound in sonic crystals. *Nat. Phys.* **13**, 369–374 (2017).
366. He, C. et al. Acoustic topological insulator and robust one-way sound transport. *Nat. Phys.* **12**, 1124–1129 (2016).
367. Fruchart, M. et al. Soft self-assembly of Weyl materials for light and sound. *Proc. Natl Acad. Sci. USA* **115**, E3655–E3664 (2018).
368. Fruchart, M., Zhou, Y. & Vitelli, V. Dualities and non-Abelian mechanics. *Nature* **577**, 636–640 (2020).
369. Fruchart, M., Yao, C. & Vitelli, V. Systematic generation of Hamiltonian families with dualities. *Phys. Rev. Res.* **5**, 023099 (2023).
370. Lei, Q.-L., Tang, F., Hu, J.-D., Ma, Y.-q & Ni, R. Duality, hidden symmetry, and dynamic isomerism in 2D hinge structures. *Phys. Rev. Lett.* **129**, 125501 (2022).
371. Yang, Z.-J. & Wang, Y.-Z. Non-abelian mechanics of elastic waves in kagome metamaterials with internal microstructures. *Proc. R. Soc. A* **479**, 20220713 (2023).
372. Zhou, D., Zhang, L. & Mao, X. Topological boundary floppy modes in quasicrystals. *Phys. Rev. X* **9**, 021054 (2019).
373. Kane, C. L. & Lubensky, T. C. Topological boundary modes in isostatic lattices. *Nat. Phys.* **10**, 39–45 (2013).
374. McInerney, J., Chen, B. G.-g, Theran, L., Santangelo, C. D. & Rocklin, D. Z. Hidden symmetries generate rigid folding mechanisms in periodic origami. *Proc. Natl Acad. Sci. USA* **117**, 30252–30259 (2020).

375. Czajkowski, M. & Rocklin, D. Z. Duality and sheared analytic response in mechanism-based metamaterials. *Phys. Rev. Lett.* **132**, 068201 (2024).
376. Gonella, S. Symmetry of the phononic landscape of twisted kagome lattices across the duality boundary. *Phys. Rev. B* **102**, 140301 (2020).
377. Danawe, H., Li, H., Al Ba'ba'a, H. & Tol, S. Existence of corner modes in elastic twisted kagome lattices. *Phys. Rev. B* **104**, L241107 (2021).
378. Azizi, P., Sarkar, S., Sun, K. & Gonella, S. Dynamics of self-dual kagome metamaterials and the emergence of fragile topology. *Phys. Rev. Lett.* **130**, 156101 (2023).
379. Allein, F. et al. Strain topological metamaterials and revealing hidden topology in higher-order coordinates. *Nat. Commun.* **14**, 6633 (2023).
380. Chen, Y., Kadic, M. & Wegener, M. Roton-like acoustical dispersion relations in 3D metamaterials. *Nat. Commun.* **12**, 3278 (2021).
381. Bossart, A. & Fleury, R. Extreme spatial dispersion in nonlocally resonant elastic metamaterials. *Phys. Rev. Lett.* **130**, 207201 (2023).
382. Kazemi, A. et al. Drawing dispersion curves: band structure customization via nonlocal phononic crystals. *Phys. Rev. Lett.* **131**, 176101 (2023).
383. Moore, D., Sambles, J., Hibbins, A., Starkey, T. & Chaplain, G. Acoustic surface modes on metasurfaces with embedded next-nearest-neighbor coupling. *Phys. Rev. B* **107**, 144110 (2023).
384. Chaplain, G., Hooper, I., Hibbins, A. & Starkey, T. Reconfigurable elastic metamaterials: engineering dispersion with beyond nearest neighbors. *Phys. Rev. Appl.* **19**, 044061 (2023).
385. Iglesias Martínez, J. A. et al. Experimental observation of roton-like dispersion relations in metamaterials. *Sci. Adv.* **7**, eabm2189 (2021).
386. Wang, K., Chen, Y., Kadic, M., Wang, C. & Wegener, M. Nonlocal interaction engineering of 2D roton-like dispersion relations in acoustic and mechanical metamaterials. *Commun. Mater.* **3**, 35 (2022).
387. Zhu, Z. et al. Observation of multiple rotons and multidirectional roton-like dispersion relations in acoustic metamaterials. *New J. Phys.* **24**, 123019 (2022).
388. Chen, Y. et al. Phonon transmission through a nonlocal metamaterial slab. *Commun. Phys.* **6**, 75 (2023).
389. Chen, Y. et al. Observation of chirality-induced roton-like dispersion in a 3D micropolar elastic metamaterial. *Adv. Funct. Mater.* **34**, 2302699 (2023).
390. Carr, S. et al. Twistronics: manipulating the electronic properties of two-dimensional layered structures through their twist angle. *Phys. Rev. B* **95**, 075420 (2017).
391. Oudich, M., Kong, X., Zhang, T., Qiu, C. & Jing, Y. Engineered moiré photonic and phononic superlattices. *Nat. Mater.* **23**, 1169–1178 (2024).
392. López, M. R., Peñaranda, F., Christensen, J. & San-Jose, P. Flat bands in magic-angle vibrating plates. *Phys. Rev. Lett.* **125**, 214301 (2020).
393. Deng, Y. et al. Magic-angle bilayer phononic graphene. *Phys. Rev. B* **102**, 180304 (2020).
394. Gardezi, S. M., Pirie, H., Carr, S., Dorrell, W. & Hoffman, J. E. Simulating twistronics in acoustic metamaterials. *2D Mater.* **8**, 031002 (2021).
395. Martí-Sabaté, M. & Torrent, D. Dipolar localization of waves in twisted phononic crystal plates. *Phys. Rev. Appl.* **15**, L011001 (2021).
396. López, M. R., Zhang, Z., Torrent, D. & Christensen, J. Theory of holey twistsonic media. *Commun. Mater.* **3**, 99 (2022).
397. Rosa, M. I., Ruzzene, M. & Prodan, E. Topological gaps by twisting. *Commun. Phys.* **4**, 130 (2021).
398. Wu, S.-Q. et al. Higher-order topological states in acoustic twisted Moiré superlattices. *Phys. Rev. Appl.* **17**, 034061 (2022).
399. Yang, Y. et al. Demonstration of negative refraction induced by synthetic gauge fields. *Sci. Adv.* **7**, eabj2062 (2021).
400. Hu, G., Krasnok, A., Mazor, Y., Qiu, C.-W. & Alù, A. Moiré hyperbolic metasurfaces. *Nano Lett.* **20**, 3217–3224 (2020).
401. Yves, S., Peng, Y.-G. & Alù, A. Topological Lifshitz transition in twisted hyperbolic acoustic metasurfaces. *Appl. Phys. Lett.* **121**, 122201 (2022).
402. Han, C. et al. Nonlocal acoustic Moiré hyperbolic metasurfaces. *Adv. Mater.* **36**, e2311350 (2024).
403. Yves, S., Galiffi, E., Ni, X., Renzi, E. M. & Alù, A. Twist-induced hyperbolic shear metasurfaces. *Phys. Rev. X* **14**, 021031 (2024).
404. Han, C. et al. Observation of dispersive acoustic quasicrystals. *Nat. Commun.* **16**, 1988 (2025).
405. Han, C. et al. All-angle unidirectional flat-band acoustic metasurfaces. *Nat. Commun.* **16**, 634 (2025).
406. Bachelard, N. et al. Emergence of an enslaved phononic bandgap in a non-equilibrium pseudo-crystal. *Nat. Mater.* **16**, 808–813 (2017).
407. Engheta, N. Four-dimensional optics using time-varying metamaterials. *Science* **379**, 1190–1191 (2023).
408. Bourdeloux, C., Fink, M. & Lemoult, F. Solution to the cocktail party problem: a time-reversal active metasurface for multipoint focusing. *Phys. Rev. Appl.* **21**, 054039 (2024).
409. Marchetti, M. C. et al. Hydrodynamics of soft active matter. *Rev. Mod. Phys.* **85**, 1143–1189 (2013).
410. Baconnier, P. et al. Self-aligning polar active matter. *Rev. Mod. Phys.* **97**, 015007 (2025).
411. Henkes, S., Fily, Y. & Marchetti, M. C. Active jamming: self-propelled soft particles at high density. *Phys. Rev. E* **84**, 040301 (2011).
412. Baconnier, P. et al. Selective and collective actuation in active solids. *Nat. Phys.* **18**, 1234–1239 (2022).
413. Gu, F., Guiselin, B., Bain, N., Zuriguel, I. & Bartolo, D. Emergence of collective oscillations in massive human crowds. *Nature* **638**, 112–119 (2025).
414. Jiao, P., Mueller, J., Raney, J. R., Zheng, X. & Alavi, A. H. Mechanical metamaterials and beyond. *Nat. Commun.* **14**, 6004 (2023).
415. Zhang, X., Zangeneh-Nejad, F., Chen, Z.-G., Lu, M.-H. & Christensen, J. A second wave of topological phenomena in photonics and acoustics. *Nature* **618**, 687–697 (2023).
416. Yang, Y. et al. Non-Abelian physics in light and sound. *Science* **383**, eadf9621 (2024).
417. Szameit, A. & Rechtsman, M. C. Discrete nonlinear topological photonics. *Nat. Phys.* **20**, 905–912 (2024).
418. Galiffi, E. et al. Extreme light confinement and control in low-symmetry phonon-polaritonic crystals. *Nat. Rev. Mater.* **9**, 9–28 (2024).
419. Ueda, H. et al. Chiral phonons in quartz probed by X-rays. *Nature* **618**, 946–950 (2023).
420. Li, N. et al. Colloquium: Phononics: manipulating heat flow with electronic analogs and beyond. *Rev. Mod. Phys.* **84**, 1045–1066 (2012).
421. Li, H. et al. Twisted moiré conductive thermal metasurface. *Nat. Commun.* https://doi.org/10.1038/s41467-024-46247-2 (2024).
422. Ronellenfitsch, H., Stoop, N., Yu, J., Forrow, A. & Dunkel, J. Inverse design of discrete mechanical metamaterials. *Phys. Rev. Mater.* **3**, 095201 (2019).
423. Mao, Y., He, Q. & Zhao, X. Designing complex architectured materials with generative adversarial networks. *Sci. Adv.* **6**, eaaz4169 (2020).
424. Van Mastrigt, R., Dijkstra, M., Van Hecke, M. & Coulais, C. Machine learning of implicit combinatorial rules in mechanical metamaterials. *Phys. Rev. Lett.* **129**, 198003 (2022).
425. Bastek, J.-H., Kumar, S., Telgen, B., Glaesener, R. N. & Kochmann, D. M. Inverting the structure–property map of truss metamaterials by deep learning. *Proc. Natl Acad. Sci. USA* **119**, e2111505119 (2022).
426. Oudich, M., Gerard, N. J., Deng, Y. & Jing, Y. Tailoring structure-borne sound through bandgap engineering in phononic crystals and metamaterials: a comprehensive review. *Adv. Funct. Mater.* **33**, 2206309 (2023).
427. Maurizi, M. et al. Designing metamaterials with programmable nonlinear responses and geometric constraints in graph space. *Nat. Mach. Intell.* **7**, 1023–1036 (2025).
428. Villar, S., Hogg, D. W., Storey-Fisher, K., Yao, W. & Blum-Smith, B. Scalars are universal: equivariant machine learning, structured like classical physics. *Adv. Neur. Inf. Proc. Syst.* **34**, 28848–28863 (2021).
429. Carminati, R., Sáenz, J. J., Greffet, J.-J. & Nieto-Vesperinas, M. Reciprocity, unitarity, and time-reversal symmetry of the S matrix of fields containing evanescent components. *Phys. Rev. A* **62**, 012712 (2000).
430. Mahaux, C. & Weidenmüller, H. *Shell Model Approach to Nuclear Reactions* (North-Holland, 1969).
431. Zirnstein, H.-G., Refael, G. & Rosenow, B. Bulk–boundary correspondence for non-Hermitian Hamiltonians via Green functions. *Phys. Rev. Lett.* **126**, 216407 (2021).

Acknowledgements

A.A. and S.Y. were supported by the National Science Foundation Science and Technology Center 'New Frontiers of Sound', the Department of Defense and the Simons Foundation. G.S. acknowledges funding by the European Union (ERC, EXCEPTIONAL, project no. 101045494). Views and opinions expressed are, however, those of the authors only and do not necessarily reflect those of the European Union or the European Research Council Executive Agency. Neither the European Union nor the granting authority can be held responsible for them. M.R.H. acknowledges support from Office of Naval Research under award no. N00014-23-1-2660. R.F. acknowledges funding by the Swiss National Science Foundation under the Eccellenza Award 181232. M.F. and V.V. acknowledge partial support from the France Chicago Center through a FACCTS grant. V.V. acknowledges partial support from the Army Research Office under grant W911NF-22-2-0109 and W911NF-23-1-0212, the National Science Foundation through the Center for Living Systems (grant no. 2317138), the National Institute for Theory and Mathematics in Biology, the Chan Zuckerberg Foundation and the Simons Foundation.

Author contributions

All authors contributed substantially to the discussion of the content. A.A. and M.R.H. initiated the project. S.Y., M.F., R.F., G.S. and V.V. researched the data and wrote the respective sections of the article. All authors reviewed and edited the manuscript.

Competing interests

The authors declare no competing interests.

Additional information

Peer review information *Nature Reviews Materials* thanks Guancong Ma, who co-reviewed with Xulong Wang; Baile Zhang; and the other, anonymous, reviewer(s) for their contribution to the peer review of this work.